


# Precision tracking of massive black hole spin evolution with LISA

Geraint Pratten <sup>1,2,\*</sup> Patricia Schmidt <sup>1,2,†</sup> Hannah Middleton <sup>1,2,‡</sup> and Alberto Vecchio <sup>1,2,§</sup>

<sup>1</sup>*School of Physics and Astronomy, University of Birmingham, Edgbaston, Birmingham, B15 2TT, United Kingdom*

<sup>2</sup>*Institute for Gravitational Wave Astronomy, University of Birmingham, Edgbaston, Birmingham, B15 2TT, United Kingdom*

(Dated: July 28, 2023)

The Laser Interferometer Space Antenna (LISA) will play a vital role in constraining the origin and evolution of massive black holes throughout the Universe. In this study we use a waveform model (IMRPhenomXPHM) that includes both precession and higher multipoles, and full Bayesian inference to explore the accuracy to which LISA can constrain the binary parameters. We demonstrate that LISA will be able to track the evolution of the spins – magnitude and orientation – to percent accuracy, providing crucial information on the dynamics and evolution of massive black hole binaries and the galactic environment in which the merger takes place. Such accurate spin-tracking further allows LISA to measure the recoil velocity of the remnant black hole to better than  $100 \text{ km s}^{-1}$  (90% credibility) and its direction to a few degrees, which provides additional important astrophysical information on the post-merger association. Using a systematic suite of binaries, we showcase that the component masses will be measurable at the sub-percent level, the sky area can be constrained to within  $\Delta\Omega_{90} \approx 0.01 \text{ deg}^2$ , and the binary redshift to less than 0.01.

## I. INTRODUCTION

The Laser Interferometer Space Antenna (LISA) will allow us to observe the mHz gravitational-wave (GW) spectrum. One of the key science goals of the mission is to trace the origin, evolution, and merger history of massive black hole (MBHs) throughout the Universe [1–3], where  $M \sim 10^4 - 10^9 M_\odot$ . These sources will be detected with large signal-to-noise ratios (SNR), allowing us to precisely measure the mass and spin angular momenta of the constituent black holes.

The population properties of the massive black hole binaries (MBHBs) that will be detected by LISA depends on a wide range of possible evolutionary pathways. Observing and characterising this population will provide vital insight into black hole seed formation, galaxy assembly, and the formation and evolution of structure throughout the Universe [1, 3–6]. Whilst there are numerous open issues, there are several mechanisms that are of key importance but are still dominated by large theoretical and observational uncertainties. For example, we have a comparatively poor understanding of the mechanisms that generate the initial black hole seeds at high redshift ( $z \gtrsim 15$ ) and the mechanisms that drive formation of the first protogalaxies. This, in turn, leads to a large uncertainty in the anticipated detection rates and the underlying astrophysical population properties [1, 2, 7].

MBHs are known to reside in the centres of galaxies, e.g. [8–17], and there is evidence that some galaxies contain a MBH, even at the early cosmological times probed at high redshift [18–20]. Coupled with the hierarchical assembly of galaxies through repeated mergers [21–24], it

is anticipated that LISA will observe numerous MBHBs across a wide range of cosmic epochs. However, there is huge uncertainty on our understanding of the astrophysical mechanisms that produced the initial seeds from which they grew. Did they originate from the collapse of heavy population III stars forming in low-metallicity environments (light seeds) [25–27] or from the collapse of large proto-galactic disks (heavy seeds) [28–33]? How did these black holes (BHs) subsequently grow? Accretion is an inevitable process and plays a key role in the growth of MBHBs [4, 34, 35]. However, there are other mechanisms that can drive the growth of MBHBs, such as repeated hierarchical mergers [5, 36–38]. Observations of MBHBs by LISA will provide us with a unique opportunity to tackle these questions and to constrain the evolutionary pathways responsible for the MBHBs observed today.

For a binary of MBHBs to merge, efficient mechanisms that dissipate the angular momentum of the system are required. Consequently, our current understanding of massive BH evolution can be broadly divided into distinct phases that are characterized by the astrophysical mechanisms driving angular momentum loss in the binary. The initial phase is primarily driven by dynamical friction caused by the gravitational interaction between the BHs and the surrounding gas and stellar material. Within this phase, the BHs are driven from a separation of approximately  $\sim \mathcal{O}(10^{-2} \text{ Mpc})$  to  $\sim \mathcal{O}(1 \text{ pc})$  [39]. Below these separations, the dominant mechanism is hardening [39–41]. Hardening refers to the interaction of fast-orbiting stellar objects and the MBHB, resulting in energy being removed from the system. If the galactic host is sufficiently gas rich, a high-density circumbinary disk can form, leading to additional hardening of the binary through viscous dissipation [42–44]. At scales below the hardening separation, e.g. [45], GW emission becomes the dominant mechanism driving the inspiral of the binary [46]. However, depending on the physical properties of the BHs, and the environment of their galactic hosts, the astrophysical mechanisms at play can be widely dif-

\* [g.pratten@bham.ac.uk](mailto:g.pratten@bham.ac.uk)

† [p.schmidt@bham.ac.uk](mailto:p.schmidt@bham.ac.uk)

‡ [hannahm@star.sr.bham.ac.uk](mailto:hannahm@star.sr.bham.ac.uk)

§ [av@star.sr.bham.ac.uk](mailto:av@star.sr.bham.ac.uk)

ferent.

A key tracer of the astrophysical formation mechanism will be the spin magnitude and orientation of the progenitor MBHs [1, 2, 24, 47–51], though these can be extremely challenging to measure [52]. The orientation of the spin, in particular, is considered a key observable to discriminate between astrophysical formation pathways. When the BH spins are not aligned with the orbital angular momentum, they induce relativistic spin *precession*, a phenomena that drives the time evolution of the spins and the orbital plane, leaving characteristic imprints in the emitted GW signal, see Sec. III.

Of particular interest is the role of the BH spins during the phase of disc-driven migration. Notably, the spin orientations of the BHs by the time they reach the GW driven regime will be sensitive to whether the galactic environment is gas-rich or gas-poor.

If the environment is gas-rich, the inspiral of the binary can lead to the formation of a cavity in the circumbinary disc with accretion onto the BHs leading to the formation of minidisks around each BH [53–57]. If the viscous minidisks are misaligned with respect to the BH spin, then Lense-Thirring precession (see [58]) will cause the inner disc to warp and dynamically relax, eventually reaching a coplanar configuration. This phenomenon is known as the Bardeen-Petterson effect [48, 59–63]. However, the efficiency of Lense-Thirring precession is limited to the Bardeen-Petterson radius, beyond which the outer disc may maintain its original misalignment. A consequence, first noted in [64], is that the outer disc will drive the secular alignment of the BH spin with the total orbital angular momentum of the disc itself. This process occurs on a longer timescale than the warping of the minidisc but on a faster timescale than the growth of the BH, i.e. we can treat the mass and spin of the BH as being fixed [65, 66]. As such, BH spins that are preferentially aligned with the orbital angular momentum are thought to be a clear tracer for the Bardeen-Petterson effect which, in turn, would suggest a gas-rich galactic host [67–69]. Conversely, MBH mergers in gas-poor environments are not expected to undergo any such alignment and we would expect the spin orientations to be generically oriented. If the spins are preferentially aligned, we are de-facto reducing the amount of precession in the binary relative to the generically oriented configurations. Spin precession is therefore a key observable in unraveling astrophysical formation pathways and will provide valuable insights into the environment of the galactic host.

A caveat to the discussion above can occur due to the torque on the disc induced by a companion BH. These torques can lead to the break-up of the disc and potentially result in BH spins that are misaligned, even in gas-rich environments [69–72]. A consequence is that this could introduce degeneracies between the environment and BH spin orientations [69].

Massive binaries, such as those discussed above, will have large signal-to-noise ratios in LISA, even at high redshift. For these binaries, we anticipate precision con-

straints on the masses and spins of the constituent BHs. Early pioneering work, see [73], demonstrated the importance of spin-precession in breaking parameter degeneracies and in improving the precision to which the binary parameters could be constrained. This work was subsequently expanded in a series of papers, e.g. [74–77], that explored the impact of higher-order PN corrections, especially higher-order spin-orbit and spin-spin terms. Two particularly important conclusions are that the modulations in the GW signal induced by spin-precession allow one to accurately measure the BH spins and that precession also breaks the degeneracy between the binary orientation and its position on the sky, which could have important implications for identifying potential EM counterparts, e.g. [78–80].

LISA is sensitive to the entire sky, with the sensitivity depending on the source location and polarization, e.g. [81]. The detector orbits the Sun such that its barycenter varies on a timescale of approximately one year. For long duration signals, the detector’s translational motion induces a Doppler shift in the observed GW signal, which is sensitive to the angular position of the source [81]. LISA also precesses around the normal to the ecliptic, leading to amplitude and phase modulations in the observed signal due to time-dependent variations in the antenna response pattern. The modulations of  $h_+$  and  $h_\times$  depend on both the sky-location and orientation of the binary [81]. Moreover, information on the angular position is encoded in the relative amplitudes and phases of the polarizations. Incorporating higher multipoles into the waveform model used to analyse the data will break parameter degeneracies, notably the degeneracy between the distance and the inclination. By accurately modelling higher multipoles, a more precise determination of the angular position and distance, e.g. see [82, 83] for the context of MBHB in LISA.

When the spin angular momenta  $\mathbf{S}_i$  are misaligned with the orbital angular momentum  $\mathbf{L}$ , precession occurs in the orbital plane and the spin vectors [84, 85]. This results in characteristic amplitude and phase modulations in the gravitational-wave signal, leading to several important observations. For example, in simple precession, the relative orientations of  $\mathbf{L}$  and  $\mathbf{S}_i$  precess about the total angular momentum  $\mathbf{J}$  [84], causing time-dependent changes in the binary’s inclination  $\iota$ , the polarization angle  $\psi$ , and the BH spins. The precession cycle’s timescale is longer than the orbital timescale but typically shorter than the LISA timescale, depending on the masses and spins of the black holes. As a consequence, precession-induced modulations enrich the gravitational-wave signal with valuable information about the binary and allow us to further break parameter degeneracies [73–75, 86–88]. The importance of precession in this context was first highlighted in the pioneering work of [73] and subsequently refined in [74–77, 89].

In this paper, we revisit the Bayesian parameter estimation of precessing MBHBs using a state-of-the-art inspiral-merger-ringdown (IMR) waveform models, IM-

RPhenomXPHM [90–92]. We use two canonical massive BH binary configurations and systematically assess the ability of LISA to resolve the individual BH parameters, including their component masses and spin-angular momenta. Previous analyses have typically relied on either inspiral-only Fisher analyses, e.g. [1, 73–77, 80, 93], or have been restricted to aligned-spins, e.g. [80, 82, 94–97].

We find broad agreement in the precision to which binary parameters are measured compared to the inspiral-only analyses, e.g. [1, 73–75]. We demonstrate the ability of LISA to accurately constrain the spin orientation hours before merger and can provide tight constraints on the the kick velocity and orientation of the remnant BH.

## II. LISA DATA ANALYSIS

### A. Time-Delay Interferometry

Here, we broadly follow [82, 98] to produce the LISA time-delay interferometry (TDI) response. In this framework, we apply a delay  $d(t)$  to a signal  $h(t)$  followed by a modulation  $F(t)$  which, in the notation of [98], can be written as

$$h_d(t) = h(t + d(t)), \quad (1)$$

$$s(t) = F(t) h_d(t). \quad (2)$$

The Fourier transform of the signal can then be written in terms of a transfer function  $\mathcal{T}$

$$\tilde{s}(f) = \mathcal{T}(f) \tilde{h}(f), \quad (3)$$

$$= \int df' \tilde{h}(f - f') \tilde{G}(f - f', f'). \quad (4)$$

Following [98], the transfer function can be decomposed into a set of signal-dependent timescales that correspond to different physical effects. The first timescale of interest is

$$T_f^2 = \frac{1}{4\pi^2} \left| \frac{d^2\varphi}{df^2} \right|, \quad (5)$$

which can be shown to reduce to the radiation-reaction timescale when the stationary phase approximation (SPA) holds [82]

$$T_f^{\text{SPA}} = \frac{1}{\sqrt{2\dot{\omega}(t_f^{\text{SPA}})}}, \quad (6)$$

where  $\omega$  is the orbital phase of the binary. This naturally leads to a time-frequency correspondence of

$$t_{\ell m}(f) = t_c - \frac{1}{2\pi} \frac{d\varphi_{\ell m}(f)}{df}, \quad (7)$$

where  $t_c$  denotes the coalescence time of the binary. The

effect of higher-order phase corrections to the transfer function can be written in terms of the time-frequency map as [98, 99]

$$\mathcal{T}_{\text{phase}}(f) = \sum_{p \geq 0} \frac{1}{p!} \left( \frac{i}{8\pi^2} \frac{d^2\varphi}{df^2} \right)^p \left( \frac{\partial^{2p}}{\partial t^{2p}} G \right) (f, t_{\ell m}(f)), \quad (8)$$

where  $G$  denotes a frequency-dependent kernel [98]. This expansion is related to the shifted uniform asymptotics expansion (SUA) introduced in [99, 100]. In this study, we focus on the leading order approximation, i.e.  $p = 1$ , and defer a detailed analysis of the impact of higher-order corrections to the transfer function to future work.

The second key timescales arises from amplitude corrections beyond the leading order [98]

$$(T_{A_p})^p = \frac{1}{(2\pi)^p} \frac{1}{A(f)} \left| \frac{d^p A}{df^p} \right|, \quad (9)$$

which leads to a transfer function of the form [98]

$$\mathcal{T}_{\text{amp}}(f) = \sum_{p \geq 0} \frac{1}{p!} (T_{A_p})^p (\partial_t^p G)(f, t_f). \quad (10)$$

Here we incorporate amplitude corrections up to second order, i.e.  $p = 2$ .

In practice, the TDI response is constructed in terms of a frequency-dependent transfer function acting on a set of waveform modes

$$h_{\ell m}^{\text{A,E,T}} = \mathcal{T}^{\text{A,E,T}}(f, t_{\ell m}(f)) h_{\ell m}(f). \quad (11)$$

The modes are generated using the precessing, higher-multipole inspiral-merger-ringdown model IMRPhenomXPHM [90–92]. The term  $\mathcal{T}^{\text{A,E,T}}(f, t_{\ell m}(f))$  denotes the TDI transfer function and  $\{A, E, T\}$  the 1G TDI channels, which are related to the original 1G Michelson TDI variables  $\{X, Y, Z\}$  by [101, 102]

$$A = \frac{1}{\sqrt{2}}(Z - X), \quad (12)$$

$$E = \frac{1}{\sqrt{6}}(X - 2Y + Z), \quad (13)$$

$$T = \frac{1}{\sqrt{3}}(X + Y + Z). \quad (14)$$

One of the key advantages of using the  $\{A, E, T\}$  variables is that they form a set of noise-orthogonal variables [101]. As such, we assume that the noise in each channel is uncorrelated resulting in a diagonalized noise matrix that simplifies the resulting analysis [102]. Note that the original variables introduced in [101] were constructed from the Sagnac variables  $\{\alpha, \beta, \gamma\}$  and are therefore slightly different from the definition adopted here and in recent work, e.g. see the discussion in [93, 103]. Finally,

we note that in order to generate the  $\{X, Y, Z\}$  TDI variables, we adopt the rigid adiabatic approximation (RAA) [98, 104], in which

$$\tilde{X}_{1.5G}(f) \approx (1 - e^{-4\pi i f L}) \tilde{X}_{\text{RAA}}(f), \quad (15)$$

where  $L = 2.5 \times 10^9 \text{m}$  is the mean LISA armlength.

### B. Bayesian Inference

A central aim of Bayesian inference is to reconstruct the posterior distribution  $p(\boldsymbol{\theta}|d)$  for the source parameters  $\boldsymbol{\theta}$  given data  $d$ . From Bayes' theorem we have

$$p(\boldsymbol{\theta}|d) = \frac{\mathcal{L}(d|\boldsymbol{\theta})\pi(\boldsymbol{\theta})}{\mathcal{Z}}, \quad (16)$$

where  $\mathcal{L}$  denotes the likelihood of the data given the parameters  $\boldsymbol{\theta}$ ,  $\pi$  the prior distributions for  $\boldsymbol{\theta}$ , and  $\mathcal{Z}$  the evidence. We perform Bayesian inference using a coherent analysis of the full LISA TDI output,  $d = \{d_j; j = A, E, T\}$ , using the `Balrog` code. In particular, we employ nested sampling [105, 106] as implemented by `Dynesty` [107, 108]. The likelihood of the data  $d$  given a set of binary parameters  $\boldsymbol{\theta}$  is [109]

$$\ln \mathcal{L}(d|\boldsymbol{\theta}) = - \sum_j \frac{\langle d_j - h_j(\boldsymbol{\theta}) | d_j - h_j(\boldsymbol{\theta}) \rangle_j}{2} + \text{const}, \quad (17)$$

where  $h_j$  denotes the TDI output for channel  $j$  produced by the GW signal. The noise weighted inner product is defined by

$$\langle a|b \rangle_j = 2 \int_0^\infty df \frac{\tilde{a}(f)\tilde{b}^*(f) + \tilde{a}^*(f)\tilde{b}(f)}{S_j(f)}, \quad (18)$$

where  $\tilde{a}(f)$  denotes the Fourier transform of the time series  $a(t)$  and  $S_j(f)$  denotes the noise power spectral density (PSD) of the  $j$ -th TDI channel. We use the noise spectral densities provided by the ESA Science Requirements Document [110, 111] and include the unresolved galactic confusion noise according to the analytical fit of [112]. As in [83], we adopt a low-frequency cut-off of  $f_{\text{low}} = 10^{-4} \text{Hz}$ , corresponding to the pessimistic scenario in which LISA only retains sensitivity over the frequency window specified in the mission design requirements [110, 111]. Any sensitivity at lower frequencies will help improve the constraints on measured parameters, so our results can be interpreted as a lower bound on the LISA science performance. Finally, we adopt the zero-noise approximation such that  $\tilde{n}(f) = 0$ , noting that the noise still enters the likelihood in Eq. (17) through the PSD. We also assume that the PSD is constant over the observation duration, though in reality we would expect the PSD to be non-stationary and to vary slowly in time, e.g. [113].

## III. MEASURING PRECESSION

### A. Black Hole Spins and Precession

Spin-induced precession is a unique and exciting phenomena that arises in the general-relativistic two-body problem [84, 85, 114–116]. If the black hole spins are misaligned with the orbital angular momentum,  $\mathbf{L}$ , spin-orbit and spin-spin couplings induce *precession*. The spin-orbit couplings drive a time-dependent evolution of the orbital plane, i.e. the direction of  $\mathbf{L}$ , whereas the relativistic spin-spin couplings, which first enter at 2PN, induce a torque on the spin-angular momenta that results in the *nutation* of  $\mathbf{L}$ , e.g. [84, 85]. The time evolution of  $\mathbf{L}$  can be decomposed into terms corresponding to precession and a term driven by radiation reaction

$$\frac{d\mathbf{L}}{dt} = \frac{d\hat{\mathbf{L}}}{dt} L + \frac{dL}{dt} \hat{\mathbf{L}}, \quad (19)$$

$$= \underbrace{(\boldsymbol{\Omega}_L \times \mathbf{L})}_{\text{precession}} L + \underbrace{\frac{dL}{dt}}_{\text{radiation reaction}} \hat{\mathbf{L}}. \quad (20)$$

Here  $\boldsymbol{\Omega}_L$  denotes the spin precession frequency in terms of a contribution arising from each of the BH spins

$$\boldsymbol{\Omega}_L = \Omega_1 \boldsymbol{\chi}_1 + \Omega_2 \boldsymbol{\chi}_2, \quad (21)$$

where the contribution to the precession frequency from each spin can be written at next-to-leading order in terms of the effective aligned spin [116–118]

$$\chi_{\text{eff}} = \frac{\boldsymbol{\chi}_1 \cdot \mathbf{L} + q \boldsymbol{\chi}_2 \cdot \mathbf{L}}{1 + q} \quad (22)$$

as [117, 119]

$$\Omega_1 = \frac{M^2}{2r^3(1+q)^2} \left( 4 + 3q - \frac{3q\chi_{\text{eff}}}{(1+q)} \frac{M^2}{L} \right), \quad (23)$$

$$\Omega_2 = \frac{qM^2}{2r^3(1+q)^2} \left( 4q + 3 - \frac{3q\chi_{\text{eff}}}{(1+q)} \frac{M^2}{L} \right), \quad (24)$$

where  $q = m_2/m_1 \leq 1$  is the mass ratio of the binary.

The dynamical effects that govern quasi-circular precessing binaries evolve on three distinct timescales. The orbital timescale is governed by  $t_{\text{orb}} \propto (r/M)^{3/2}$ , the precession timescale  $t_{\text{prec}} \propto (r/M)^{5/2}$  [84, 85], and the radiation reaction timescale by  $t_{\text{rad}} \propto (r/M)^4$ . At large separations,  $r \gg M$ , the timescales obey a hierarchy

$$t_{\text{orb}} \ll t_{\text{prec}} \ll t_{\text{rad}}. \quad (25)$$

In the context of LISA, we expect MBH of total mass  $\sim 10^4 - 10^7 M_\odot$  to be observable for  $\mathcal{O}(\text{days})$  to  $\mathcal{O}(\text{years})$ , meaning that the binaries can undergo a comparatively large number of precession cycles compared to current

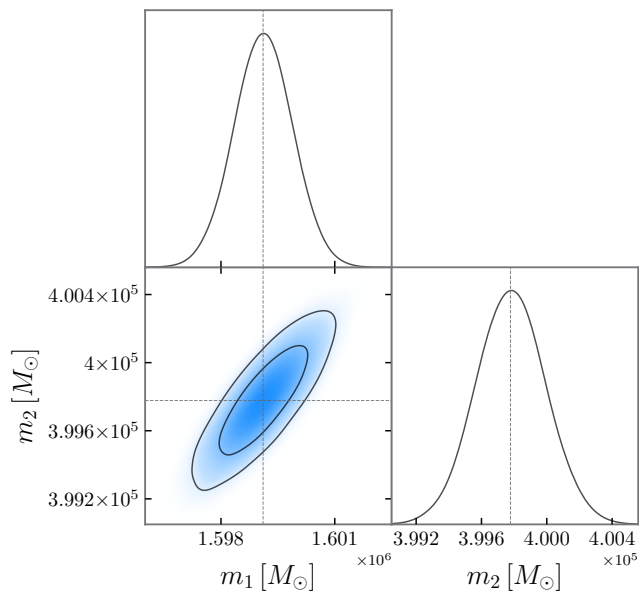


FIG. 1. Corner plot showing the joint posteriors on the source frame component masses. The mass of the primary BH is measured to within  $\mathcal{O}(10^3 M_\odot)$  and the mass of the secondary to  $\mathcal{O}(10^2 M_\odot)$ .

ground-based observations of stellar mass black holes [120–122]. Therefore, we can anticipate that MBHB observations with LISA will provide valuable opportunities for precision measurements of black hole spins and a comprehensive understanding of their evolution over multiple precession cycles.

## B. Constraining Binary Parameters and Early Warning

In this study, we focus on a systematic series of investigations centred on two MBHBs that correspond to a low-spin (LS) and a high-spin (HS) configuration respectively. For each configuration, we consider three different inclination angles for the binary  $\theta_{\text{JN}}$  and three different spin tilt angles  $\cos \theta_i = \vec{\chi}_i \cdot \mathbf{L}$ . The three spin tilts chosen correspond to a series of binaries in which the primary spin is approximately i) aligned with  $\mathbf{L}$ , ii) perpendicular to  $\mathbf{L}$ , and iii) anti-aligned with  $\mathbf{L}$ . See Tables I and II in App. A for further details. Throughout this paper, we adopt HS2 as a canonical binary configuration, corresponding to a high-spin binary with  $\chi_1 = 0.8$ ,  $\chi_2 = 0.6$ ,  $\iota = 42$  degrees,  $\theta_1 = 21$  degrees and  $\theta_2 = 31.4$  degrees. Throughout this work, we keep the redshift of the binaries the same,  $z = 3$ , as well as the detector-frame (i.e. redshifted) masses, corresponding to  $6.4 \times 10^6 M_\odot$  and  $1.6 \times 10^5 M_\odot$ <sup>1</sup>.

Even at a redshift of  $z \approx 3$ , the set of binaries considered here have large signal-to-noise-ratio  $\rho \approx \mathcal{O}(10^3)$  resulting in excellent constraints on the BH masses and spins, irrespective of the orientation of the binary  $\theta_{\text{JN}}$  or the orientation of the primary BH spin  $\theta_1$ . As in other recent studies of MBHBs, e.g. [82, 83, 124], we find that the individual masses are resolved to  $\Delta m_i \approx \mathcal{O}(0.1\%)$ , as shown in Fig. 1.

For both the high- and low-spin binaries, we broadly find that the spin magnitude of the primary is measured to an error on the order of  $\Delta \chi_1 \approx \mathcal{O}(0.1\%)$ , the secondary spin magnitude to  $\Delta \chi_2 \approx \mathcal{O}(1\%)$ , the primary tilt to within  $\Delta \theta_1 \approx \mathcal{O}(1\%)$ , and the secondary tilt to  $\Delta \theta_2 \approx \mathcal{O}(5\%)$ , as shown in Fig. 2 for the high-spin series and Fig. 7 in the Appendix for the low-spin series. A full list of recovered parameters and their 90% credible intervals can be found in Tab III. As we are able to resolve the spin magnitudes and orientations to exquisite precision, there is no need to rely on effective spin parameterizations, such as those proposed in [119, 125].

Finally, we provide an assessment of the precision to which LISA can constrain the sky localization of the binary system when using an IMR waveform model that incorporates spin precession. For all binaries, the measurement accuracy for the ecliptic longitude is approximately  $\Delta l \approx \mathcal{O}(0.05\%)$ , while the ecliptic latitude is constrained to  $\Delta b \approx \mathcal{O}(1\%)$ . Furthermore, the inclination angle is determined to a precision of  $\Delta \theta_{\text{JN}} \approx \mathcal{O}(0.1\%)$ , and the redshift to approximately  $\approx \mathcal{O}(0.1\%)$ . For the luminosity distance, we find that the distance to the binaries can be measured to with  $\Delta d_L \approx \mathcal{O}(0.01 \text{ Gpc})$  which, assuming a Planck18 cosmology [123], translates to  $\Delta z \approx \mathcal{O}(0.01)$ .

These measurement accuracies correspond to a 90% credible sky area of  $\Delta \Omega_{90} \approx \mathcal{O}(0.01 \text{ deg}^2)$  and a 90% confidence sky localization volume of  $\Delta V_{90} \approx 7 \times 10^{-4} \text{ Gpc}^3$ . In contrast to [83], which used an aligned-spin model, our findings indicate an improvement in the angular resolution of LISA due to the incorporation of spin precession, in agreement with previous studies [73–75]. The complete sky localization posteriors are shown in Fig. 3. The accuracy to which we can constrain the sky location and distance plays a critical role in determining the multi-messenger prospects, e.g see the recent detailed study in [126] which outlines the number and properties of EM-bright signals that will be observable in both LISA and a subset of EM facilities.

Finally, we note that the sky localization we report above is based on the analysis of the complete data from when it first enters the LISA band at  $f_{\text{low}} \approx 10^{-4} \text{ Hz}$  through to merger. In reality, the binary could be detectable before merger, depending on how the SNR accumulates. If a binary can be detected in sufficiently low-latency, then a preliminary skymap could be produced using partial data, e.g. adapting the methodology of [127], followed by a skymap generated using the complete data. As shown in Fig. 4, the SNR rapidly accumulates and passes a detection threshold, arbitrarily taken to be  $\rho_{\text{det}} \approx 12$ , on the order of 150 hours be-

<sup>1</sup> We adopt the Planck18 cosmology throughout this paper [123].

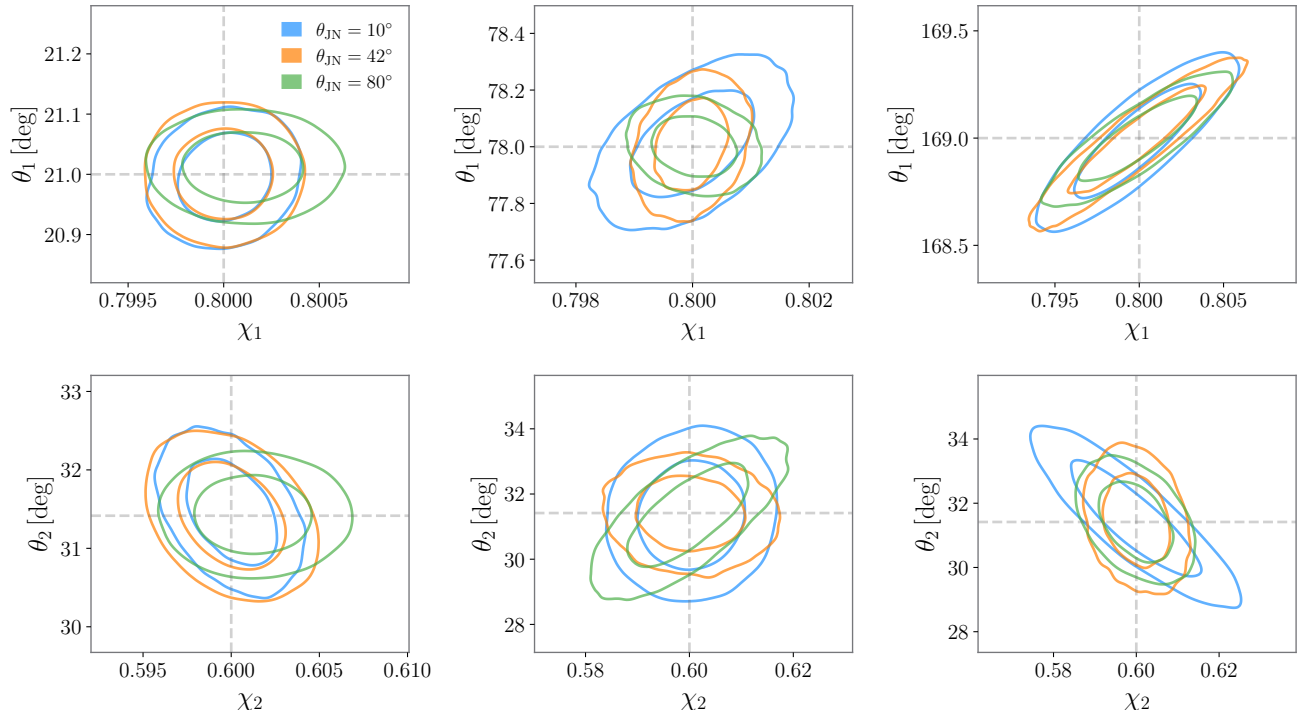


FIG. 2. Constraints on the spin magnitude and orientations for the high-spin series. The top row corresponds to the primary (heavier) BH and the bottom row the secondary (lighter) BH. The left-most panels depict a configuration where the primary spin is approximately aligned with  $\mathbf{L}$ , the middle panels a highly-precessing configuration, and the right-most panels where  $\chi_1$  is approximately anti-aligned with  $\mathbf{L}$ . For each configuration, we consider three orientations that approximately correspond to: face-on (blue), edge-on (orange), and face-off (green) binaries.

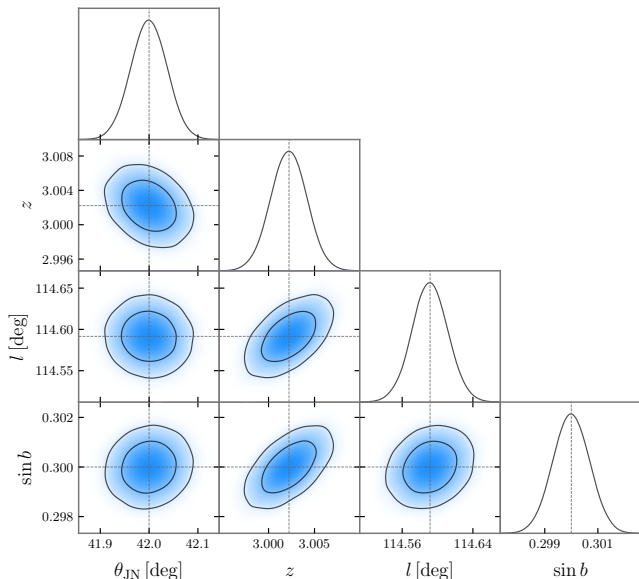


FIG. 3. Corner plot showing the sky localization, redshift  $z$ , and the polar inclination angle of the binary  $\iota$  in degrees.

fore merger. This would provide ample time to request a

protected LISA science data period to ensure the merger is recorded based on the current lead time estimate of  $\approx 2$  days [128]. Note, however, that we do not make any attempt to tackle challenges pertaining to the low-latency detection and localization of these binaries on the  $\approx \mathcal{O}(\text{hrs})$  timescale.

### C. Constraining Spin Evolution

In gas-rich environments, the binary can undergo a gas driven migration phase until the viscous timescales become smaller than the gravitational radiation-reaction timescale. At later stages of the inspiral, the binary evolution will be driven by GW emission. For the binaries considered here, the initial separation  $r_i = r(f_{\text{low}})$  is within the GW-dominated phase and we can neglect disk-migration effects on the evolution. In addition, we note that if one assumes that the total angular momentum of the binary is preferentially aligned with the circumbinary disk, then the spin tilt angles  $\theta_i$  are equivalent to those inherited from the gas-driven migration, see recent work in [69, 129–132].

We therefore evolve the binary from an initial separation  $r_i$  to a final separation of  $r_f = 5M$  using an orbit-

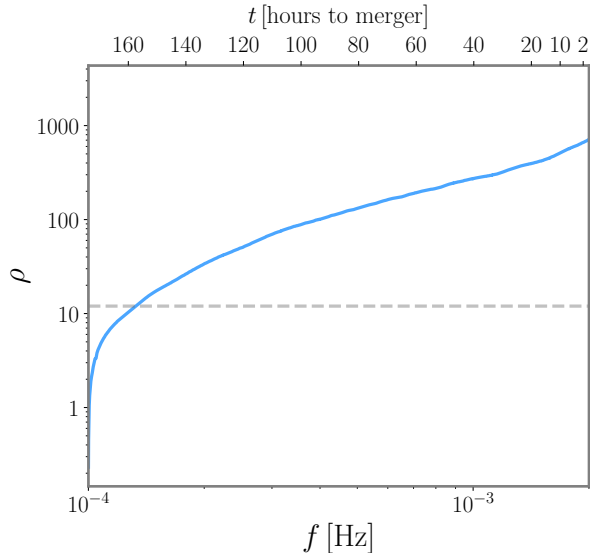


FIG. 4. Growth of the signal-to-noise ratio (SNR) as a function of frequency or, equivalently, the time to merger (in hours). The horizontal dashed line denotes  $\rho_{\text{det}} = 12$ , which we use as a proxy for the SNR at which a binary can be detected. For the canonical binary considered here, the system is visible up to  $\approx 150$  hours before merger.

averaged post-Newtonian evolution [133, 134]. The spin tilt angles of each BH are constrained to 1 degree or better which, when combined with the stringent mass constraints at the 0.01% level, allows for a precise determination of the evolution of the individual BH spins. LISA will have the capability to accurately ascertain the magnitudes and orientations of the spins at a comparable level of precision, down to approximately 1 hour before the merger, as depicted in Fig. 5. As we shall see in the next section, detailed knowledge of the spin orientations at merger is vital if we are to accurately infer the recoil velocity and orientation. Finally, in the bottom panel of Fig. 5 we show the contributions of each spin  $\Omega_i$  to the precession frequency  $\Omega_L$ , as defined in Eqns. (21) - (24). Precession has been measured in binary pulsars with typical precession frequencies being on the order of  $10^{-10}$  Hz, e.g. [135–139]. For the MBHs considered here, the precession frequencies fall in the mHz regime.

#### D. Constraining Remnant Properties

As is well known, GWs carry energy and angular momentum away from the system, driving the inspiral of the binary. The orbit shrinks until the two BHs eventually plunge and form a single, perturbed BH. The emission of GWs transfers linear momentum away from the binary, causing a displacement to its center of mass in the opposite direction [140–143]. However, the loss of linear

momentum through the merger is asymmetric and imparts a net linear velocity, i.e. a *recoil* or a *kick*, onto the remnant BH [144–150]. The magnitude and orientation of the recoil has important astrophysical implications, with the first evidence for large recoil velocities being recently reported [150]. This mechanism can displace or even eject BHs from the galactic center [151], potentially influencing the evolution of the MBH and its host galaxy [152, 153]. Recoils approaching  $10^3 \text{ km s}^{-1}$  could have a velocity that exceeds the escape velocity of the galactic host [151, 154], suppressing the fraction of galaxies that host a central MBH [155, 156], which has implications for the estimated event rates in LISA [3, 157, 158].

If a MBH is surrounded by a circumbinary disk, the perturbations to the gas induced by a recoiling BH can potentially give rise to an EM counterpart [159–166]. The detectability of the EM counterpart is expected to depend significantly on the kick velocity of the recoiling BH and, potentially, to the orientation relative to the circumbinary disk. For the signal to be observable, a large recoil velocity on the order of  $\mathcal{O}(10^3 \text{ km s}^{-1})$  would be necessary. Kick velocities closer to  $\mathcal{O}(10^2 \text{ km s}^{-1})$  are unlikely to produce an observable EM counterpart, based on current theoretical models [165]. The EM emission spectra will be highly reliant on the specific manner in which the disk undergoes shocks [166]. Joint GW-EM inference will allow us to build a comprehensive understanding of the astrophysical processes at play in MBHB mergers. LISA will be able to accurately measure the masses and spins of the BHs as it approaches the merger, providing vital information on the geometry of the binary.

In order to understand the accuracy with which we can infer the remnant properties, we evolve the spins from  $f_{\text{low}}$  through to the merger, as above, and use the NR calibrated fits of [167] to estimate the mass  $M_f$  of the remnant BH, the magnitude of the kick velocity  $|v_f|$ , and the orientation of the kick velocity  $\theta_{v_f}$ . For the canonical binary we have focused on here, we find a moderate kick velocity of  $|v_f| \approx 575 \text{ km s}^{-1}$  with an orientation of  $\theta_{v_f} \approx 165 \text{ deg}$ , as shown in the top right panel of Fig. 6. The top left panel of Fig. 6 highlight the precision to which LISA will be able to resolve the binary geometry in terms of the orientations of  $\hat{J}$ ,  $\hat{\chi}_1$ ,  $\hat{\chi}_2$ , and  $\hat{v}_f$ . As discussed in [167], these quantities are defined in an instantaneous frame in which the total orbital angular momentum  $\hat{L}_{\text{orb}}$  points along  $\hat{z}$  at a reference time of  $t = -100M$ . Whilst a kick velocity of  $v_f \approx 575 \text{ km s}^{-1}$  is likely to be too small to result in an EM-bright signal [166], the detection and accurate characterisation of the BH recoil through GW observations alone will allow us to place important constraints on the underlying astrophysical processes. See also the discussion in [66], which explores differential misalignment and the implications for the kick velocity. As discussed in [66], kick velocities on the order of  $\approx 1500 \text{ km s}^{-1}$  can be produced in highly spinning binaries, with larger kick velocities only being anticipated for comparable mass BHs due to the dynamical alignment of the BH spins. The bottom panel

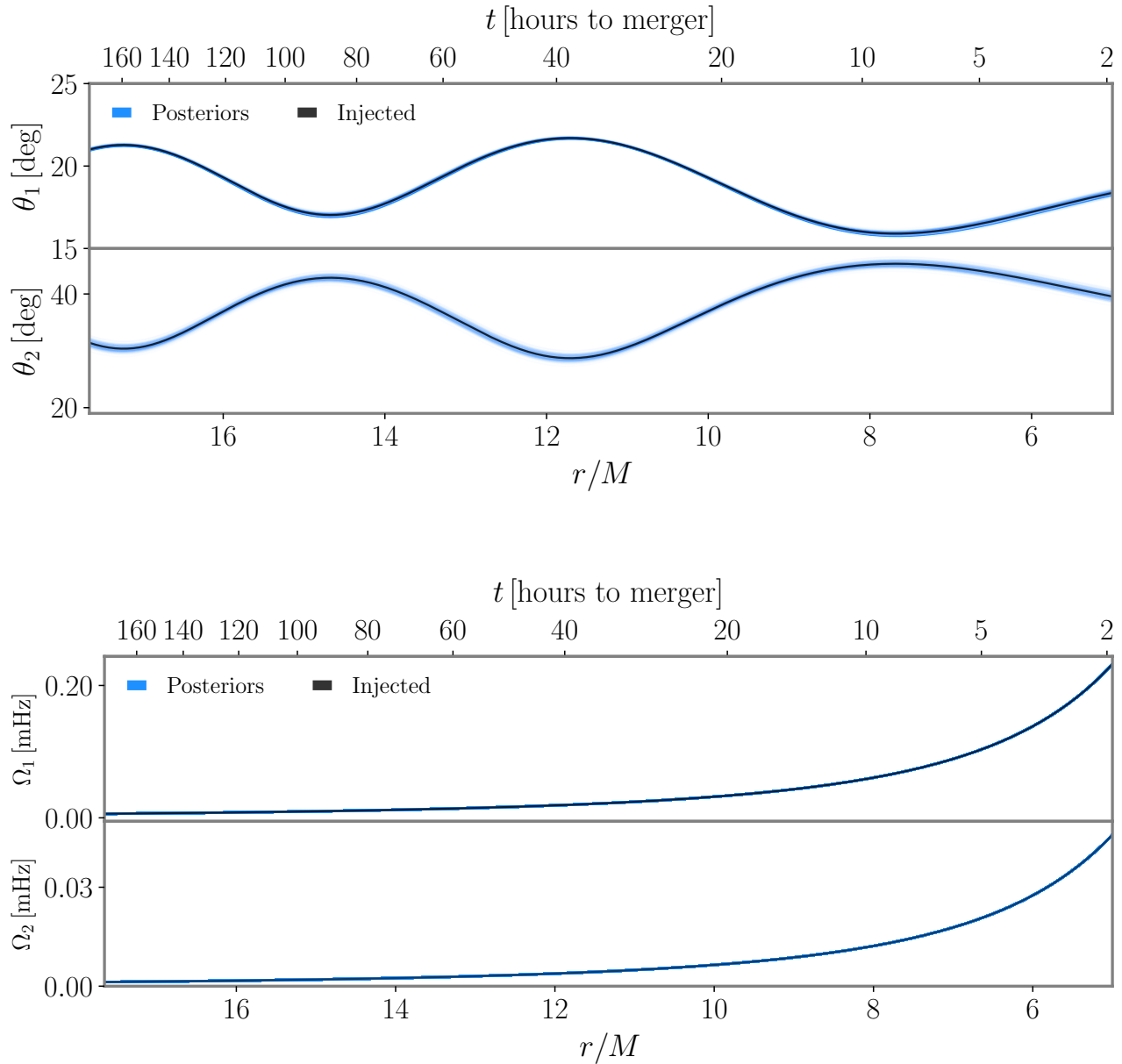


FIG. 5. Tracking precession of binary HS2. Top panel: Posterior distributions on the spin evolution from the initial binary separation defined by the starting frequency of  $f_{\text{low}} = 10^{-4}$  Hz down to a separation of  $r = 5M$ , where we terminate the PN integration. On the top axis, we show the approximate time to merger in days, noting that we are considering a MBHB with a total redshifted mass of  $M_z = 8 \times 10^6 M_\odot$  or, equivalently, a source-frame mass of  $M_{\text{src}} = 2 \times 10^6 M_\odot$ . As noted in [83], a binary of this mass is expected to emit GWs in the LISA band for  $\tau \approx 6$  days. Bottom panel: Posterior distributions on the evolution of the spin precession frequencies  $\Omega_i$  in Hz as defined in Eq. (21). Towards the end of the inspiral, the primary BH has a precession frequency  $\mathcal{O}(20 \text{ mHz})$  and the secondary BH  $\mathcal{O}(0.5 \text{ mHz})$ .

of Fig. 6 shows the posterior distributions on the kick velocity as a function of the tilt of the primary spin at  $t = -100M$  for all configurations in the HS series. For the binaries in which the primary spin is essentially orthogonal to  $\hat{L}$ , the approaches a maximum on the order of  $|v_f| \approx 1200 \text{ km s}^{-1}$ .

#### IV. CONCLUSIONS AND FUTURE WORK

In this work, we have revisited the Bayesian parameter estimation of MBHBs in LISA using a state-of-the-art inspiral-merger-ringdown waveform model that incorporates both precession and higher multipoles [90–92]. A



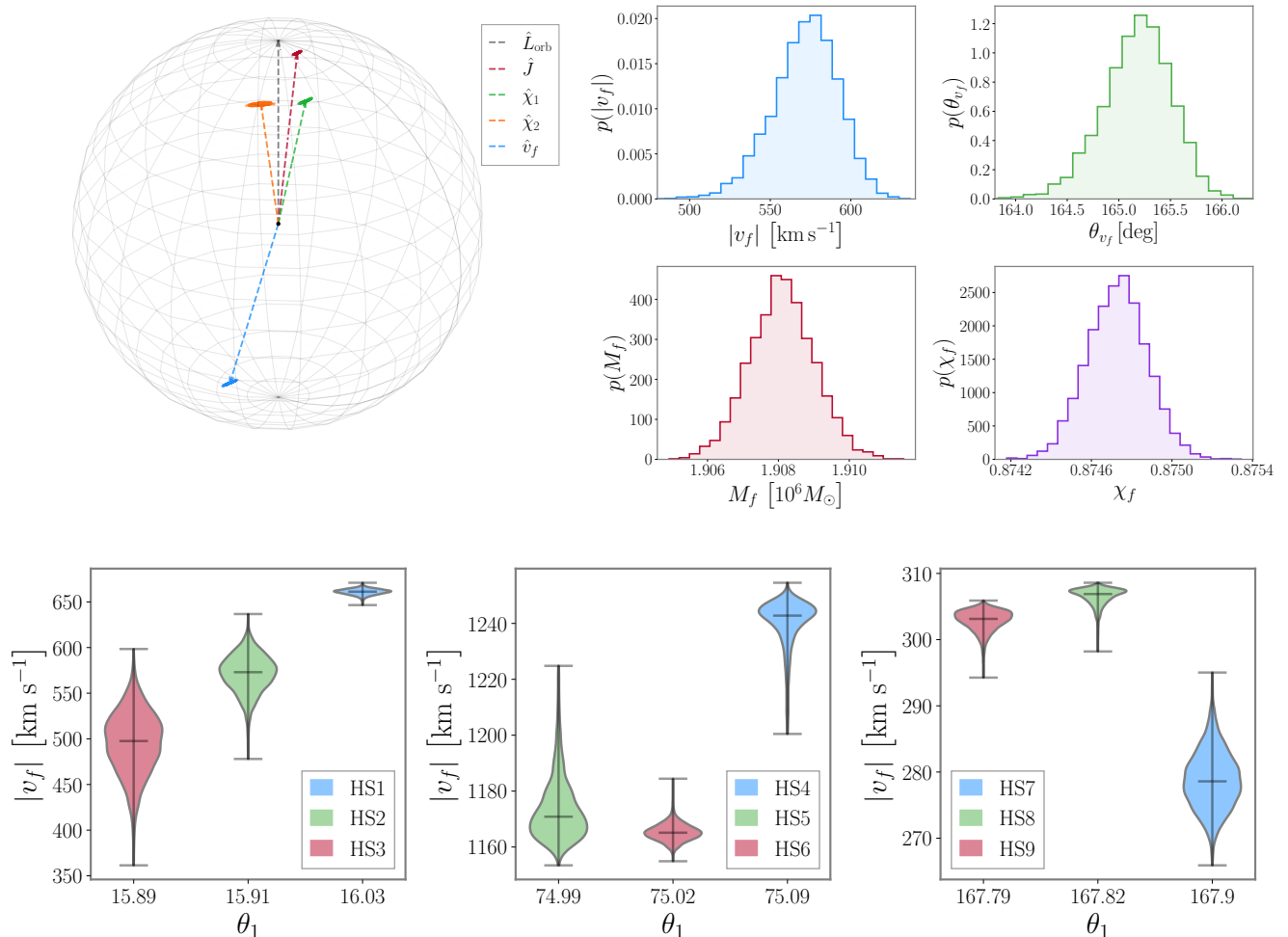


FIG. 6. The top panels refer to the canonical “HS2” binary configuration. Top left: Posterior distributions for normalized total angular momentum and the dimensionless spin vectors of each BH. All quantities are defined in the orbital angular momentum frame  $\hat{L} = \hat{z}$  at  $t = -100M$  [167]. Top right: Posterior distributions for the magnitude of the kick velocity  $v_f$ , the polar angle of the kick orientation, the remnant source-frame BH mass  $M_f$ , and the dimensionless BH spin  $\chi_f$ . The bottom panels show the effect of different geometrical spin configurations for the “high spin binary” on the posterior distributions for the magnitude of the kick velocity  $v_f$ . Here  $\theta_1$  is the polar angle of the primary spin defined at a time  $t = -100M$ , as used to estimate the recoil velocity.

key focus was to investigate LISA’s capability to accurately constrain the masses and spins of MBHs using the complete GW signal. Given the precision to which LISA can resolve the individual spin magnitudes and orientations, we highlighted how LISA will be able to accurately track the evolution of the BH spins through to the merger. An important consequence is that LISA will be able to accurately predict the magnitude and orientation of the recoil velocity, a key observable in exploring potential EM-bright counterparts to MBH mergers.

In addition to the intrinsic parameters, we also demonstrated that, irrespective of the binary geometry, LISA will be able to constrain the sky location and orientation of the binary to sub-percent level, event out to a redshift

of  $z \approx 3$ , at least for the subset of binaries considered here. A detailed study exploring a larger population of MBHBs is underway to explore the broader parameter space and the concomitant implications for joint GW-EM analyses.

The detection rate of MBHBs is anticipated to be sensitive to the astrophysical distribution of spin magnitudes and orientations, especially for heavy binaries with  $M > 10^7 M_\odot$ . Detecting and inferring the properties of these binaries will play a critical role in understanding the astrophysical origin and evolution of MBHs throughout the Universe. This also has important implications in exploring the complex interplay between the MBH population observed by LISA and the stochastic

GW background observed by PTAs, for which significant evidence has now been observed [168–174]. In a recent paper, [175] demonstrated the implications of observing this PTA background on the anticipated detection rate of MBHBs in LISA. Although [175] focused on a systematic suite of non-spinning binaries, the framework can be expanded to incorporate MBHBs with generically oriented spins, as explored here.

Detailed modeling of spin-precession plays a crucial role in resolving parameter degeneracies and enhancing the precision with which we can measure binary parameters [73, 74, 87–89]. It also plays a vital role in exploring MBH formation channels and constraining the astrophysics that drives their mergers. However, an important issue that remains unaddressed here is that of waveform systematics. The stringent accuracy requirements for future waveform models, necessary to reach this level of precision, pose immense challenges for source modelling. Recent developments, such as those in [176–182], have shown progress in enhancing the accuracy of the current generation of waveform models. Yet, achieving the accuracy *and* data analysis demands of LISA still remains a significant endeavor. In future work, we will explore the impact of waveform systematics on our ability to constrain the astrophysics behind MBH mergers. Moreover, we note that the GW signal can be influenced by environmental effects, such as dynamical friction or torquing from angular momentum exchange between accretion discs and the binary [183–186]. Detailed phenomenological modeling of environmental effects opens a promising avenue to discern the astrophysical processes at play in galactic nuclei but could introduce systematic biases into our analysis [187].

The results presented here are a first step towards integrating waveform models with precession and higher multipoles into a global fit pipeline. Notably, [97] has demonstrated the application of aligned-spin phenomenological waveform models to address the MBHB aspect of the global fit. In our case, we have employed IMRPhenomXPHM to perform Bayesian inference on individual MBHBs. Finally, we note that IMRPhenomXPHM can be effectively combined with the heterodyned likelihood [188], even when including precession and higher multipoles [189]. In forthcoming work, we will build upon the findings presented here to demonstrate how MBHBs can effectively constrain the underlying astrophysical population [190] and facilitate tests of General Relativity [191].

## ACKNOWLEDGMENTS

We thank Clément Bonnerot and Jean-Baptiste Bayle for useful comments on the manuscript. GP gratefully acknowledges support from a Royal Society University Research Fellowship URF\R1\221500 and RF\ERE\221015. PS and GP acknowledge support from STFC grant ST/V005677/1. HM and AV acknowledge the support of the UK Space Agency Grant No.

ST/V002813/1 and ST/X002071/1. AV acknowledges the support of the Royal Society and Wolfson Foundation. Computations were performed on the University of Birmingham’s high performance computing service Blue-BEAR and the Bondi HPC Cluster at the Birmingham Institute for Gravitational Wave Astronomy. Parts of this analysis made use of `numpy` [192], `matplotlib` [193], `scipy` [194], `numpy` [192], `GetDist` [195], `precession` [133, 134], and `dynesty` [108].

## Appendix A: Binaries

ID	$m_1$	$m_2$	$\chi_1$	$\chi_2$	$\theta_1$	$\theta_2$	$\phi_{12}$	$z$	$\iota$	$b$	$l$
	[ $10^6 M_\odot$ ]				[deg]				[deg]		
LS1	1.6	0.4	0.2	0.4	21.0	31.4	34.4	3.0	10.0	17.5	114.6
LS2	–	–	–	–	–	–	–	–	42.0	–	–
LS3	–	–	–	–	–	–	–	–	80.0	–	–
LS4	1.6	0.4	0.2	0.4	78.0	31.4	34.4	3.0	10.0	17.5	114.6
LS5	–	–	–	–	–	–	–	–	42.0	–	–
LS6	–	–	–	–	–	–	–	–	80.0	–	–
LS7	1.6	0.4	0.2	0.4	169.0	31.4	34.4	3.0	10.0	17.5	114.6
LS8	–	–	–	–	–	–	–	–	42.0	–	–
LS9	–	–	–	–	–	–	–	–	80.0	–	–

TABLE I. Summary table for the *low spin* (LS) binaries, characterized by  $\chi_1 = 0.2$  and  $\chi_2 = 0.4$ . We consider three configurations, corresponding to  $\theta_1 = \{21^\circ, 78^\circ, 169^\circ\}$  degrees respectively. For each configuration, we consider three inclination angles  $\iota = \{10^\circ, 42^\circ, 80^\circ\}$  to gauge the impact of the binary orientation on our ability to resolve the binary parameters. Here 10 degrees corresponds to a near face-on configuration and 80 degrees to an approximately edge-on configuration. The masses correspond to the source-frame values and a dashed line denotes that the value is equivalent to the row above.

## Appendix B: Summary of Bayesian Inference

Here we list the exact configurations used for the low-spin (LS) and high-spin (HS) binaries. For each set of binaries we fix the sky-location, distance, component masses, spin magnitudes, and spin tilt of the secondary BH. We then systematically vary the spin tilt of the primary BH from an approximately aligned configuration through to an approximately anti-aligned configuration. Spins that are misaligned with the orbital angular momentum give rise to relativistic spin couplings that drive the precession of the orbital plane and the spins themselves [84, 85]. By tilting the primary spin we are effectively changing the amount of precession in the binary. In addition to varying the primary spin magnitude, we also

ID	$m_1$	$m_2$	$\chi_1$	$\chi_2$	$\theta_1$	$\theta_2$	$\phi_{12}$	$z$	$\iota$	$b$	$l$
	[ $10^6 M_\odot$ ]				[deg]				[deg]		
HS1	1.6	0.4	0.8	0.6	21.0	31.4	34.4	3.0	10.0	17.5	114.6
HS2	–	–	–	–	–	–	–	–	42.0	–	–
HS3	–	–	–	–	–	–	–	–	80.0	–	–
HS4	1.6	0.4	0.8	0.6	78.0	31.4	34.4	3.0	10.0	17.5	114.6
HS5	–	–	–	–	–	–	–	–	42.0	–	–
HS6	–	–	–	–	–	–	–	–	80.0	–	–
HS7	1.6	0.4	0.8	0.6	169.0	31.4	34.4	3.0	10.0	17.5	114.6
HS8	–	–	–	–	–	–	–	–	42.0	–	–
HS9	–	–	–	–	–	–	–	–	80.0	–	–

TABLE II. As in Tab. I, but now for the *high spin* (HS) binaries, where  $\chi_1 = 0.8$  and  $\chi_2 = 0.6$ .

explore three binary orientations for each tilt configuration to explore the impact of observing the binary from a near face-on configuration through to a near edge-on configuration. Due to the fact that the binaries undergo multiple precession cycles after entering the observable LISA band, we find that the orientation has little impact on our ability to constrain the BH spins.

### SUPPLEMENTARY PLOTS

Figure 7 is the low-spin counterpart of Fig. 5, demonstrating that even for low spins, LISA can accurately resolve the magnitudes and orientations of BH spins to a comparable level of accuracy.

### CORNER PLOTS

The complete joint posteriors for our canonical binary configuration, HS2, are shown in Fig. 8.

TABLE III. Summary of the 90% credible intervals on the recovered parameters for all injections considered in this paper. Here HS denotes the high-spin series and LS the low-spin series. The component masses  $m_i$  correspond to the source-frame values,  $\chi_i$  the dimensionless spin magnitudes,  $\theta_i$  the spin-tilt angles, and  $\phi_{12}$  the difference in the azimuthal spin angles between the two BH spins.

ID	$m_1$ [ $10^6 M_\odot$ ]	$m_2$ [ $10^6 M_\odot$ ]	$\chi_1$ —	$\chi_2$ —	$\theta_1$ [deg]	$\theta_2$ [deg]	$\phi_{12}$ [deg]	$\theta_{\text{JN}}$ [deg]	$z$ —	$\sin b$ —	$l$ [deg]
HS1	$1.599^{+0.001}_{-0.001}$	$0.400^{+0.0003}_{-0.0003}$	$0.800^{+0.0003}_{-0.0003}$	$0.600^{+0.003}_{-0.003}$	$21.0^{+0.1}_{-0.1}$	$31.5^{+0.7}_{-0.7}$	$34.5^{+1.3}_{-1.3}$	$10.00^{+0.05}_{-0.05}$	$3.002^{+0.003}_{-0.003}$	$0.300^{+0.001}_{-0.001}$	$114.59^{+0.06}_{-0.07}$
HS2	$1.599^{+0.001}_{-0.001}$	$0.400^{+0.0004}_{-0.0003}$	$0.800^{+0.0003}_{-0.0003}$	$0.600^{+0.003}_{-0.003}$	$21.0^{+0.1}_{-0.1}$	$31.4^{+0.7}_{-0.7}$	$34.4^{+1.5}_{-1.5}$	$42.00^{+0.06}_{-0.06}$	$3.002^{+0.003}_{-0.003}$	$0.300^{+0.001}_{-0.001}$	$114.59^{+0.03}_{-0.03}$
HS3	$1.599^{+0.002}_{-0.002}$	$0.400^{+0.0005}_{-0.0005}$	$0.800^{+0.0004}_{-0.0003}$	$0.601^{+0.004}_{-0.004}$	$21.0^{+0.1}_{-0.1}$	$31.4^{+0.5}_{-0.5}$	$34.5^{+1.2}_{-1.2}$	$80.00^{+0.03}_{-0.03}$	$3.003^{+0.005}_{-0.005}$	$0.300^{+0.002}_{-0.002}$	$114.59^{+0.02}_{-0.02}$
HS4	$1.599^{+0.002}_{-0.002}$	$0.400^{+0.0005}_{-0.0006}$	$0.800^{+0.0012}_{-0.0012}$	$0.600^{+0.011}_{-0.011}$	$78.0^{+0.2}_{-0.2}$	$31.4^{+1.8}_{-1.8}$	$34.2^{+2.5}_{-2.4}$	$10.00^{+0.08}_{-0.08}$	$3.002^{+0.005}_{-0.005}$	$0.300^{+0.002}_{-0.002}$	$114.59^{+0.09}_{-0.09}$
HS5	$1.599^{+0.002}_{-0.002}$	$0.400^{+0.0006}_{-0.0006}$	$0.800^{+0.0007}_{-0.0007}$	$0.600^{+0.012}_{-0.011}$	$78.0^{+0.2}_{-0.2}$	$31.4^{+1.2}_{-1.3}$	$34.2^{+2.4}_{-2.3}$	$42.00^{+0.04}_{-0.04}$	$3.002^{+0.006}_{-0.006}$	$0.300^{+0.002}_{-0.002}$	$114.59^{+0.03}_{-0.03}$
HS6	$1.599^{+0.002}_{-0.002}$	$0.400^{+0.0005}_{-0.0005}$	$0.800^{+0.0008}_{-0.0008}$	$0.600^{+0.013}_{-0.013}$	$78.0^{+0.1}_{-0.1}$	$31.3^{+1.7}_{-1.7}$	$34.3^{+3.1}_{-3.3}$	$80.00^{+0.05}_{-0.05}$	$3.002^{+0.004}_{-0.004}$	$0.300^{+0.002}_{-0.002}$	$114.59^{+0.02}_{-0.02}$
HS7	$1.599^{+0.005}_{-0.005}$	$0.400^{+0.0012}_{-0.0012}$	$0.800^{+0.0040}_{-0.0041}$	$0.599^{+0.017}_{-0.017}$	$169.0^{+0.3}_{-0.3}$	$31.5^{+2.0}_{-1.9}$	$34.6^{+7.1}_{-7.0}$	$10.00^{+0.33}_{-0.34}$	$3.002^{+0.012}_{-0.012}$	$0.300^{+0.005}_{-0.005}$	$114.59^{+0.26}_{-0.25}$
HS8	$1.599^{+0.004}_{-0.004}$	$0.400^{+0.0011}_{-0.0011}$	$0.800^{+0.0043}_{-0.0044}$	$0.600^{+0.009}_{-0.009}$	$169.0^{+0.3}_{-0.3}$	$31.5^{+1.6}_{-1.6}$	$34.5^{+5.5}_{-5.5}$	$42.00^{+0.11}_{-0.11}$	$3.002^{+0.011}_{-0.011}$	$0.300^{+0.005}_{-0.005}$	$114.59^{+0.07}_{-0.07}$
HS9	$1.599^{+0.004}_{-0.004}$	$0.400^{+0.0011}_{-0.0011}$	$0.800^{+0.0038}_{-0.0037}$	$0.600^{+0.010}_{-0.010}$	$169.0^{+0.2}_{-0.2}$	$31.5^{+1.3}_{-1.3}$	$34.4^{+4.9}_{-4.9}$	$80.00^{+0.11}_{-0.11}$	$3.002^{+0.010}_{-0.010}$	$0.300^{+0.003}_{-0.003}$	$114.59^{+0.04}_{-0.04}$
LS1	$1.599^{+0.005}_{-0.005}$	$0.400^{+0.001}_{-0.001}$	$0.200^{+0.004}_{-0.004}$	$0.400^{+0.014}_{-0.014}$	$21.0^{+0.5}_{-0.5}$	$31.2^{+3.8}_{-3.8}$	$34.2^{+5.6}_{-6.0}$	$10.00^{+0.08}_{-0.08}$	$3.00^{+0.01}_{-0.01}$	$0.300^{+0.003}_{-0.003}$	$114.59^{+0.18}_{-0.18}$
LS2	$1.599^{+0.003}_{-0.003}$	$0.400^{+0.001}_{-0.001}$	$0.200^{+0.002}_{-0.002}$	$0.400^{+0.012}_{-0.012}$	$21.0^{+0.6}_{-0.6}$	$31.7^{+2.7}_{-2.7}$	$34.3^{+7.5}_{-8.0}$	$41.99^{+0.13}_{-0.13}$	$3.00^{+0.01}_{-0.01}$	$0.300^{+0.003}_{-0.003}$	$114.59^{+0.11}_{-0.10}$
LS3	$1.599^{+0.003}_{-0.003}$	$0.400^{+0.001}_{-0.001}$	$0.200^{+0.002}_{-0.002}$	$0.399^{+0.014}_{-0.014}$	$21.0^{+0.6}_{-0.6}$	$31.2^{+2.4}_{-2.3}$	$34.9^{+6.0}_{-6.1}$	$80.00^{+0.05}_{-0.05}$	$3.00^{+0.01}_{-0.01}$	$0.300^{+0.004}_{-0.004}$	$114.59^{+0.04}_{-0.04}$
LS4	$1.599^{+0.004}_{-0.004}$	$0.400^{+0.001}_{-0.001}$	$0.200^{+0.002}_{-0.002}$	$0.393^{+0.024}_{-0.024}$	$77.7^{+1.1}_{-1.1}$	$30.9^{+2.8}_{-3.0}$	$35.2^{+6.6}_{-6.7}$	$10.00^{+0.07}_{-0.07}$	$3.00^{+0.01}_{-0.01}$	$0.300^{+0.003}_{-0.003}$	$114.59^{+0.18}_{-0.18}$
LS5	$1.599^{+0.003}_{-0.003}$	$0.400^{+0.001}_{-0.001}$	$0.200^{+0.002}_{-0.002}$	$0.398^{+0.021}_{-0.022}$	$77.8^{+0.9}_{-0.9}$	$31.3^{+2.5}_{-2.8}$	$35.7^{+6.5}_{-6.7}$	$42.00^{+0.12}_{-0.12}$	$3.00^{+0.01}_{-0.01}$	$0.300^{+0.003}_{-0.003}$	$114.59^{+0.11}_{-0.11}$
LS6	$1.599^{+0.003}_{-0.003}$	$0.400^{+0.001}_{-0.001}$	$0.200^{+0.002}_{-0.002}$	$0.399^{+0.016}_{-0.016}$	$78.1^{+0.8}_{-0.8}$	$31.3^{+2.0}_{-2.1}$	$32.9^{+6.2}_{-6.6}$	$80.00^{+0.07}_{-0.07}$	$3.00^{+0.01}_{-0.01}$	$0.300^{+0.004}_{-0.004}$	$114.59^{+0.04}_{-0.04}$
LS7	$1.599^{+0.007}_{-0.006}$	$0.400^{+0.001}_{-0.001}$	$0.200^{+0.006}_{-0.007}$	$0.400^{+0.020}_{-0.024}$	$169.0^{+0.5}_{-0.5}$	$31.3^{+4.8}_{-3.8}$	$34.1^{+11.9}_{-14.8}$	$10.00^{+0.17}_{-0.17}$	$3.00^{+0.01}_{-0.01}$	$0.300^{+0.004}_{-0.004}$	$114.60^{+0.22}_{-0.22}$
LS8	$1.599^{+0.004}_{-0.004}$	$0.400^{+0.001}_{-0.001}$	$0.200^{+0.004}_{-0.004}$	$0.401^{+0.015}_{-0.014}$	$169.0^{+0.6}_{-0.7}$	$31.3^{+4.1}_{-3.8}$	$34.8^{+12.6}_{-12.3}$	$42.00^{+0.16}_{-0.16}$	$3.00^{+0.01}_{-0.01}$	$0.300^{+0.003}_{-0.003}$	$114.59^{+0.13}_{-0.13}$
LS9	$1.599^{+0.004}_{-0.004}$	$0.400^{+0.001}_{-0.001}$	$0.200^{+0.003}_{-0.003}$	$0.400^{+0.013}_{-0.013}$	$169.0^{+0.3}_{-0.3}$	$31.4^{+2.2}_{-2.1}$	$34.7^{+10.6}_{-11.1}$	$80.00^{+0.09}_{-0.09}$	$3.00^{+0.01}_{-0.01}$	$0.300^{+0.004}_{-0.004}$	$114.59^{+0.04}_{-0.04}$

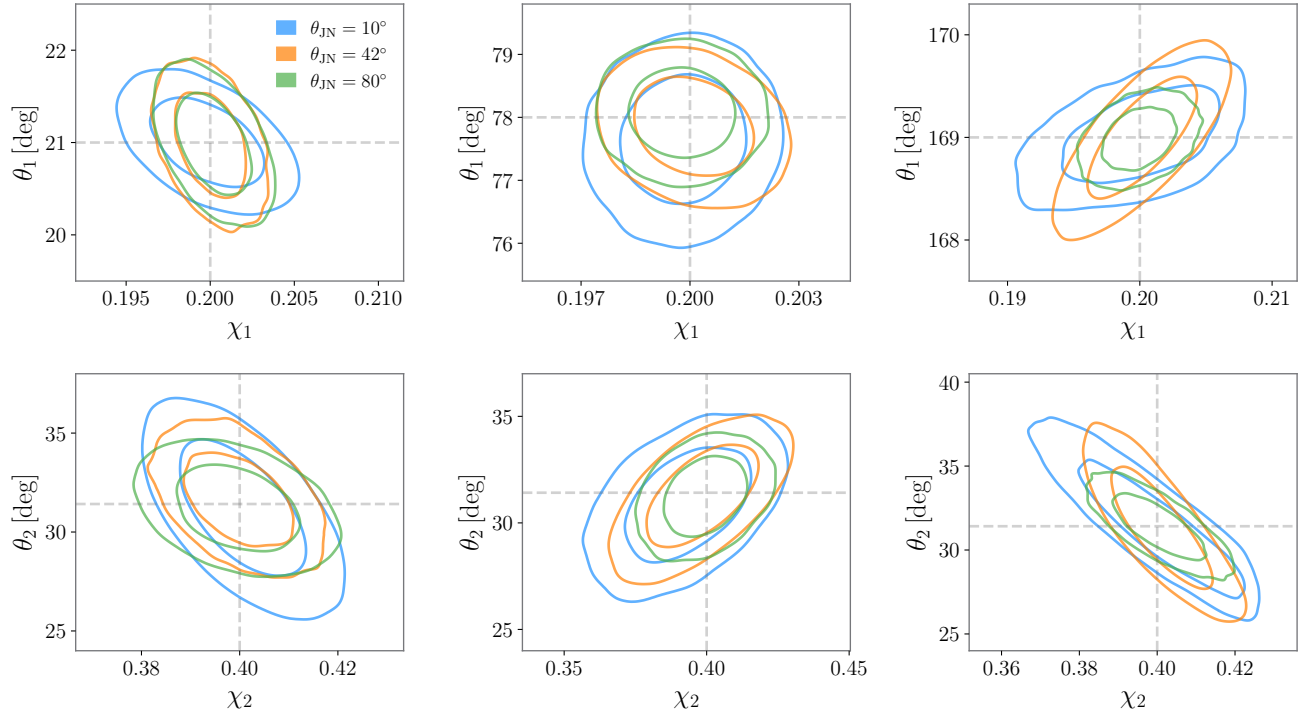


FIG. 7. As per Fig. 2 but for the low-spin systematic series.

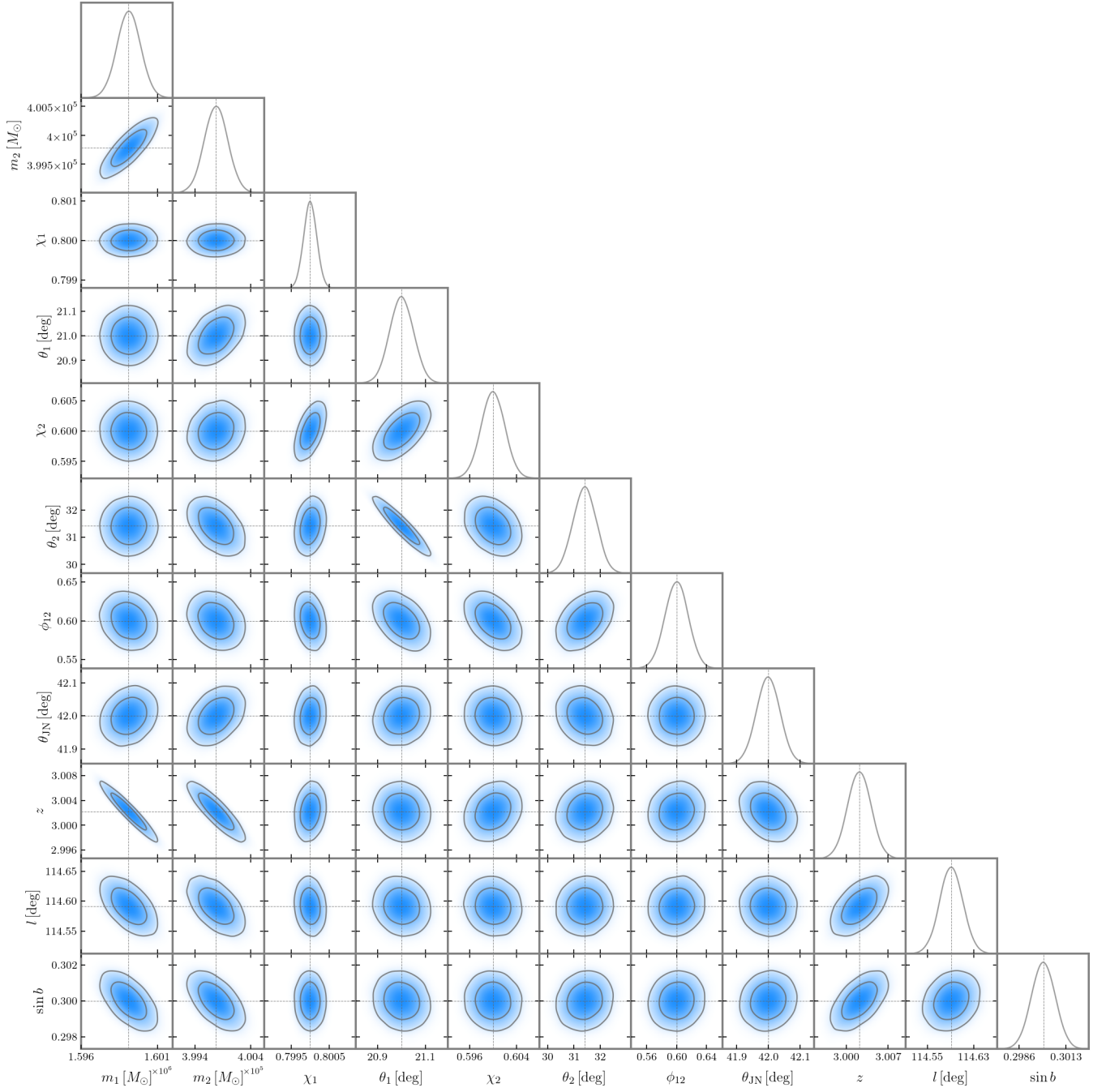


FIG. 8. Full corner plot for our canonical binary. The dashed lines denote the injected values.

- [1] Antoine Klein *et al.*, “Science with the space-based interferometer eLISA: Supermassive black hole binaries,” *Phys. Rev. D* **93**, 024003 (2016), arXiv:1511.05581 [gr-qc].
- [2] Alberto Sesana, “Black Hole Science With the Laser Interferometer Space Antenna,” *Front. Astron. Space Sci.* **8**, 601646 (2021), arXiv:2105.11518 [astro-ph.CO].
- [3] Pau Amaro-Seoane *et al.* (LISA), “Astrophysics with the Laser Interferometer Space Antenna,” *Living Rev. Rel.* **26**, 2 (2023), arXiv:2203.06016 [gr-qc].
- [4] Qing-juan Yu and Scott Tremaine, “Observational constraints on growth of massive black holes,” *Mon. Not. Roy. Astron. Soc.* **335**, 965–976 (2002), arXiv:astro-ph/0203082.
- [5] Takamitsu Tanaka and Zoltan Haiman, “The Assembly of Supermassive Black Holes at High Redshifts,” *Astrophys. J.* **696**, 1798–1822 (2009), arXiv:0807.4702 [astro-ph].
- [6] Marta Volonteri, “Formation of Supermassive Black Holes,” *Astron. Astrophys. Rev.* **18**, 279–315 (2010), arXiv:1003.4404 [astro-ph.CO].
- [7] Enrico Barausse, Irina Dvorkin, Michael Tremmel, Marta Volonteri, and Matteo Bonetti, “Massive Black Hole Merger Rates: The Effect of Kiloparsec Separation Wandering and Supernova Feedback,” *Astrophys. J.* **904**, 16 (2020), arXiv:2006.03065 [astro-ph.GA].
- [8] John Kormendy and Douglas Richstone, “Inward Bound—The Search For Supermassive Black Holes In Galactic Nuclei,” *Annual Review of Astronomy and Astrophysics* **33**, 581 (1995).
- [9] A. M. Ghez, B. L. Klein, M. Morris, and E. E. Becklin, “High proper motion stars in the vicinity of Sgr A\*: Evidence for a supermassive black hole at the center of our galaxy,” *Astrophys. J.* **509**, 678–686 (1998), arXiv:astro-ph/9807210.
- [10] Karl Gebhardt *et al.*, “A Relationship between Nuclear Black Hole Mass and Galaxy Velocity Dispersion,” *Astrophysical Journal, Letters* **539**, L13–L16 (2000), arXiv:astro-ph/0006289 [astro-ph].
- [11] Laura Ferrarese and David Merritt, “A Fundamental Relation between Supermassive Black Holes and Their Host Galaxies,” *Astrophysical Journal, Letters* **539**, L9–L12 (2000), arXiv:astro-ph/0006053 [astro-ph].
- [12] R. Schödel, T. Ott, R. Genzel, A. Eckart, N. Mouawad, and T. Alexander, “Stellar Dynamics in the Central Arcsecond of Our Galaxy,” *Astrophys. J.* **596**, 1015–1034 (2003), arXiv:astro-ph/0306214 [astro-ph].
- [13] Laura Ferrarese and Holland Ford, “Supermassive black holes in galactic nuclei: Past, present and future research,” *Space Sci. Rev.* **116**, 523–624 (2005), arXiv:astro-ph/0411247.
- [14] A. M. Ghez *et al.*, “Measuring Distance and Properties of the Milky Way’s Central Supermassive Black Hole with Stellar Orbits,” *Astrophys. J.* **689**, 1044–1062 (2008), arXiv:0808.2870 [astro-ph].
- [15] Reinhard Genzel, Frank Eisenhauer, and Stefan Gillessen, “The Galactic Center Massive Black Hole and Nuclear Star Cluster,” *Rev. Mod. Phys.* **82**, 3121–3195 (2010), arXiv:1006.0064 [astro-ph.GA].
- [16] John Kormendy and Luis C. Ho, “Coevolution (Or Not) of Supermassive Black Holes and Host Galaxies,” *Ann. Rev. Astron. Astrophys.* **51**, 511–653 (2013), arXiv:1304.7762 [astro-ph.CO].
- [17] Kazunori Akiyama *et al.* (Event Horizon Telescope), “First M87 Event Horizon Telescope Results. I. The Shadow of the Supermassive Black Hole,” *Astrophys. J. Lett.* **875**, L1 (2019), arXiv:1906.11238 [astro-ph.GA].
- [18] E. Bañados *et al.*, “Discovery of eight  $z \sim 6$  quasars from Pan-STARRS1,” *Astron. J.* **148**, 14 (2014), arXiv:1405.3986 [astro-ph.GA].
- [19] Xue-Bing Wu *et al.*, “An ultraluminous quasar with a twelve-billion-solar-mass black hole at redshift 6.30,” *Nature* **518**, 512–515 (2015), arXiv:1502.07418 [astro-ph.GA].
- [20] Eduardo Banados *et al.*, “An 800-million-solar-mass black hole in a significantly neutral Universe at redshift 7.5,” *Nature* **553**, 473–476 (2018), arXiv:1712.01860 [astro-ph.GA].
- [21] Onsi Fakhouri, Chung-Pei Ma, and Michael Boylan-Kolchin, “The merger rates and mass assembly histories of dark matter haloes in the two Millennium simulations,” *Mon. Not. R. Astron. Soc.* **406**, 2267–2278 (2010), arXiv:1001.2304 [astro-ph.CO].
- [22] Mirek Giersz, Nathan Leigh, Arkadiusz Hypki, Nora Lützgendorf, and Abbas Askar, “MOCCA code for star cluster simulations - IV. A new scenario for intermediate mass black hole formation in globular clusters,” *Mon. Not. R. Astron. Soc.* **454**, 3150–3165 (2015), arXiv:1506.05234 [astro-ph.GA].
- [23] Joseph A. O’Leary, Benjamin P. Moster, Thorsten Naab, and Rachel S. Somerville, “EMERGE: empirical predictions of galaxy merger rates since  $z \sim 6$ ,” *Mon. Not. R. Astron. Soc.* **501**, 3215–3237 (2021), arXiv:2001.02687 [astro-ph.GA].
- [24] Marta Volonteri, Mélanie Habouzit, and Monica Colpi, “The origins of massive black holes,” *Nature Reviews Physics* **3**, 732–743 (2021), arXiv:2110.10175 [astro-ph.GA].
- [25] Piero Madau and Martin J. Rees, “Massive black holes as Population III remnants,” *Astrophys. J. Lett.* **551**, L27–L30 (2001), arXiv:astro-ph/0101223.
- [26] Alexander Heger, C. L. Fryer, S. E. Woosley, N. Langer, and D. H. Hartmann, “How massive single stars end their life,” *Astrophys. J.* **591**, 288–300 (2003), arXiv:astro-ph/0212469.
- [27] Shingo Hirano, Takashi Hosokawa, Naoki Yoshida, Hideyuki Umeda, Kazuyuki Omukai, Gen Chiaki, and Harold W. Yorke, “One Hundred First Stars : Protostellar Evolution and the Final Masses,” *Astrophys. J.* **781**, 60–81 (2014), arXiv:1308.4456 [astro-ph.CO].
- [28] Martin G. Haehnelt and Martin J. Rees, “The formation of nuclei in newly formed galaxies and the evolution of the quasar population,” *Mon. Not. Roy. Astron. Soc.* **263**, 168–178 (1993).
- [29] Abraham Loeb and Frederic A. Rasio, “Collapse of primordial gas clouds and the formation of quasar black holes,” *Astrophys. J.* **432**, 52 (1994), arXiv:astro-ph/9401026.
- [30] Volker Bromm and Abraham Loeb, “Formation of the first supermassive black holes,” *Astrophys. J.* **596**, 34–46 (2003), arXiv:astro-ph/0212400.

- [31] Mitchell C. Begelman, Marta Volonteri, and Martin J. Rees, “Formation of supermassive black holes by direct collapse in pregalactic halos,” *Mon. Not. Roy. Astron. Soc.* **370**, 289–298 (2006), arXiv:astro-ph/0602363.
- [32] Giuseppe Lodato and Priyamvada Natarajan, “Supermassive black hole formation during the assembly of pregalactic discs,” *Mon. Not. R. Astron. Soc.* **371**, 1813–1823 (2006), arXiv:astro-ph/0606159 [astro-ph].
- [33] Bhaskar Agarwal, Sadegh Khochfar, Jarrett L. Johnson, Eyal Neistein, Claudio Dalla Vecchia, and Mario Livio, “Ubiquitous seeding of supermassive black holes by direct collapse,” *Mon. Not. Roy. Astron. Soc.* **425**, 2854 (2012), arXiv:1205.6464 [astro-ph.CO].
- [34] Marta Volonteri and M. J. Rees, “Quasars at  $z=6$ : The survival of the fittest,” *Astrophys. J.* **650**, 669–678 (2006), arXiv:astro-ph/0607093.
- [35] Tonima Tasnim Ananna *et al.*, “The Accretion History of AGNs. I. Supermassive Black Hole Population Synthesis Model,” *Astrophys. J.* **871**, 240 (2019), arXiv:1810.02298 [astro-ph.GA].
- [36] Marta Volonteri, Francesco Haardt, and Piero Madau, “The Assembly and merging history of supermassive black holes in hierarchical models of galaxy formation,” *Astrophys. J.* **582**, 559–573 (2003), arXiv:astro-ph/0207276.
- [37] Philip F. Hopkins *et al.*, “A Unified, merger-driven model for the origin of starbursts, quasars, the cosmic x-ray background, supermassive black holes and galaxy spheroids,” *Astrophys. J. Suppl.* **163**, 1–49 (2006), arXiv:astro-ph/0506398.
- [38] Alberto Sesana, Marta Volonteri, and Francesco Haardt, “The imprint of massive black hole formation models on the LISA data stream,” *Mon. Not. Roy. Astron. Soc.* **377**, 1711–1716 (2007), arXiv:astro-ph/0701556.
- [39] J. Frank and M. J. Rees, “Effects of massive black holes on dense stellar systems,” *Mon. Not. R. Astron. Soc.* **176**, 633–647 (1976).
- [40] A. P. Lightman and S. L. Shapiro, “The distribution and consumption rate of stars around a massive, collapsed object,” *Astrophys. J.* **211**, 244–262 (1977).
- [41] Gerald D. Quinlan, “The dynamical evolution of massive black hole binaries - I. hardening in a fixed stellar background,” *New Astron.* **1**, 35–56 (1996), arXiv:astro-ph/9601092.
- [42] M. C. Begelman, R. D. Blandford, and M. J. Rees, “Massive black hole binaries in active galactic nuclei,” *Nature* **287**, 307–309 (1980).
- [43] Andrew Gould and Hans-Walter Rix, “Binary black hole mergers from planet-like migrations,” *Astrophys. J. Lett.* **532**, L29 (2000), arXiv:astro-ph/9912111.
- [44] Andres Escala, Richard B. Larson, Paolo S. Coppi, and Diego Mardones, “The Role of gas in the merging of massive black holes in galactic nuclei. 2. Black hole merging in a clumpy disk,” *Astrophys. J.* **630**, 152–166 (2005), arXiv:astro-ph/0406304.
- [45] Eugene Vasiliev, Fabio Antonini, and David Merritt, “The final-parsec problem in nonspherical galaxies revisited,” *Astrophys. J.* **785**, 163 (2014), arXiv:1311.1167 [astro-ph.GA].
- [46] P. C. Peters and J. Mathews, “Gravitational radiation from point masses in a Keplerian orbit,” *Phys. Rev.* **131**, 435–439 (1963).
- [47] Marta Volonteri, Piero Madau, Eliot Quataert, and Martin J. Rees, “The Distribution and cosmic evolution of massive black hole spins,” *Astrophys. J.* **620**, 69–77 (2005), arXiv:astro-ph/0410342.
- [48] Tamara Bogdanovic, Christopher S. Reynolds, and M. Coleman Miller, “Alignment of the spins of supermassive black holes prior to merger,” *Astrophys. J. Lett.* **661**, L147 (2007), arXiv:astro-ph/0703054.
- [49] Emanuele Berti and Marta Volonteri, “Cosmological black hole spin evolution by mergers and accretion,” *Astrophys. J.* **684**, 822–828 (2008), arXiv:0802.0025 [astro-ph].
- [50] A. Sesana, E. Barausse, M. Dotti, and E. M. Rossi, “Linking the spin evolution of massive black holes to galaxy kinematics,” *Astrophys. J.* **794**, 104 (2014), arXiv:1402.7088 [astro-ph.CO].
- [51] Davide Fiacconi, Debora Sijacki, and J. E. Pringle, “Galactic nuclei evolution with spinning black holes: method and implementation,” *Mon. Not. Roy. Astron. Soc.* **477**, 3807–3835 (2018), arXiv:1712.00023 [astro-ph.GA].
- [52] Christopher S. Reynolds, “Observing black holes spin,” *Nature Astron.* **3**, 41–47 (2019), arXiv:1903.11704 [astro-ph.HE].
- [53] C. Roedig, M. Dotti, A. Sesana, J. Cuadra, and M. Colpi, “Limiting eccentricity of subparsec massive black hole binaries surrounded by self-gravitating gas discs,” *Mon. Not. R. Astron. Soc.* **415**, 3033–3041 (2011), arXiv:1104.3868 [astro-ph.CO].
- [54] Brian D. Farris, Paul Duffell, Andrew I. MacFadyen, and Zoltan Haiman, “Binary Black Hole Accretion From a Circumbinary Disk: Gas Dynamics Inside the Central Cavity,” *Astrophys. J.* **783**, 134 (2014), arXiv:1310.0492 [astro-ph.HE].
- [55] Brian D. Farris, Paul Duffell, Andrew I. MacFadyen, and Zoltan Haiman, “Binary Black Hole Accretion During Inspiral and Merger,” *Mon. Not. Roy. Astron. Soc.* **447**, L80–L84 (2015), arXiv:1409.5124 [astro-ph.HE].
- [56] Monica Colpi, “Massive Binary Black Holes in Galactic Nuclei and Their Path to Coalescence,” *Space Sci. Rev.* **183**, 189–221 (2014), arXiv:1407.3102 [astro-ph.GA].
- [57] Dennis B. Bowen, Vassilios Mewes, Manuela Campanelli, Scott C. Noble, Julian H. Krolik, and Miguel Zilhao, “Quasi-Periodic Behavior of Mini-Disks in Binary Black Holes Approaching Merger,” *Astrophys. J. Lett.* **853**, L17 (2018), arXiv:1712.05451 [astro-ph.HE].
- [58] Josef Lense and Hans Thirring, “Ueber den Einfluss der Eigenrotation der Zentralkoerper auf die Bewegung der Planeten und Monde nach der Einsteinschen Gravitationstheorie,” *Phys. Z.* **19**, 156–163 (1918).
- [59] James M. Bardeen and Jacobus A. Petterson, “The Lense-Thirring Effect and Accretion Disks around Kerr Black Holes,” *Astrophys. J. Lett.* **195**, L65 (1975).
- [60] S. Kumar and J. E. Pringle, “Twisted accretion discs - The Bardeen-Petterson effect,” *Mon. Not. R. Astron. Soc.* **213**, 435–442 (1985).
- [61] P. A. G. Scheuer and R. Feiler, “The realignment of a black hole misaligned with its accretion disc,” *Mon. Not. R. Astron. Soc.* **282**, 291 (1996).
- [62] Priyamvada Natarajan and J. E. Pringle, “The Alignment of disk and black hole spins in active galactic nuclei,” *Astrophys. J. Lett.* **506**, L97 (1998), arXiv:astro-ph/9808187.



- [63] Philip J. Armitage and Priyamvada Natarajan, “Accretion during the merger of supermassive black holes,” *Astrophys. J. Lett.* **567**, L9–L12 (2002), [arXiv:astro-ph/0201318](#).
- [64] MARTIN J REES, “Relativistic jets and beams in radio galaxies,” *Nature* **275**, 516–517 (1978).
- [65] A. R. King and U. Kolb, “The evolution of black hole mass and angular momentum,” *Mon. Not. Roy. Astron. Soc.* **305**, 654 (1999), [arXiv:astro-ph/9901296](#).
- [66] Davide Gerosa *et al.*, “Spin alignment and differential accretion in merging black hole binaries,” *Mon. Not. Roy. Astron. Soc.* **451**, 3941–3954 (2015), [arXiv:1503.06807 \[astro-ph.GA\]](#).
- [67] M. Coleman Miller and Julian H. Krolik, “Alignment of supermassive black hole binary orbits and spins,” *Astrophys. J.* **774**, 43 (2013), [arXiv:1307.6569 \[astro-ph.HE\]](#).
- [68] Davide Gerosa *et al.*, “Multi-timescale analysis of phase transitions in precessing black-hole binaries,” *Phys. Rev. D* **92**, 064016 (2015), [arXiv:1506.03492 \[gr-qc\]](#).
- [69] Nathan Steinle and Davide Gerosa, “The Bardeen–Petterson effect, disc breaking, and the spin orientations of supermassive black hole binaries,” *Mon. Not. Roy. Astron. Soc.* **519**, 5031–5042 (2023), [arXiv:2211.00044 \[astro-ph.HE\]](#).
- [70] S. Doğan, C. J. Nixon, A. R. King, and J. E. Pringle, “Instability of warped discs,” *Mon. Not. Roy. Astron. Soc.* **476**, 1519–1531 (2018), [arXiv:1801.05426 \[astro-ph.HE\]](#).
- [71] Davide Gerosa, Giovanni Rosotti, and Riccardo Barbieri, “The Bardeen–Petterson effect in accreting supermassive black hole binaries: a systematic approach,” *Mon. Not. Roy. Astron. Soc.* **496**, 3060–3075 (2020), [arXiv:2004.02894 \[astro-ph.GA\]](#).
- [72] Rebecca Nealon *et al.*, “The Bardeen–Petterson effect in accreting supermassive black hole binaries: disc breaking and critical obliquity,” *Mon. Not. Roy. Astron. Soc.* **509**, 5608–5621 (2021), [arXiv:2111.08065 \[astro-ph.HE\]](#).
- [73] Alberto Vecchio, “LISA observations of rapidly spinning massive black hole binary systems,” *Phys. Rev. D* **70**, 042001 (2004), [arXiv:astro-ph/0304051](#).
- [74] Ryan N. Lang and Scott A. Hughes, “Measuring coalescing massive binary black holes with gravitational waves: The Impact of spin-induced precession,” *Phys. Rev. D* **74**, 122001 (2006), [Erratum: *Phys. Rev. D* **75**, 089902 (2007), Erratum: *Phys. Rev. D* **77**, 109901 (2008)], [arXiv:gr-qc/0608062](#).
- [75] Ryan N. Lang and Scott A. Hughes, “Localizing coalescing massive black hole binaries with gravitational waves,” *Astrophys. J.* **677**, 1184 (2008), [arXiv:0710.3795 \[astro-ph\]](#).
- [76] Adamantios Stavridis, K. G. Arun, and Clifford M. Will, “Precessing supermassive black hole binaries and dark energy measurements with LISA,” *Phys. Rev. D* **80**, 067501 (2009), [arXiv:0907.4686 \[gr-qc\]](#).
- [77] Ryan N. Lang, Scott A. Hughes, and Neil J. Cornish, “Measuring parameters of massive black hole binaries with partially aligned spins,” *Phys. Rev. D* **84**, 022002 (2011), [arXiv:1101.3591 \[gr-qc\]](#).
- [78] Yike Tang, Zoltán Haiman, and Andrew Macfadyen, “The late inspiral of supermassive black hole binaries with circumbinary gas discs in the LISA band,” *Mon. Not. Roy. Astron. Soc.* **476**, 2249–2257 (2018), [arXiv:1801.02266 \[astro-ph.HE\]](#).
- [79] Stéphane D’Ascoli *et al.*, “Electromagnetic Emission from Supermassive Binary Black Holes Approaching Merger,” *Astrophys. J.* **865**, 140 (2018), [arXiv:1806.05697 \[astro-ph.HE\]](#).
- [80] Alberto Mangiagli *et al.*, “Observing the inspiral of coalescing massive black hole binaries with LISA in the era of Multi-Messenger Astrophysics,” *Phys. Rev. D* **102**, 084056 (2020), [arXiv:2006.12513 \[astro-ph.HE\]](#).
- [81] Curt Cutler, “Angular resolution of the LISA gravitational wave detector,” *Phys. Rev. D* **57**, 7089–7102 (1998), [arXiv:gr-qc/9703068](#).
- [82] Sylvain Marsat, John G. Baker, and Tito Dal Canton, “Exploring the Bayesian parameter estimation of binary black holes with LISA,” *Phys. Rev. D* **103**, 083011 (2021), [arXiv:2003.00357 \[gr-qc\]](#).
- [83] Geraint Pratten *et al.*, “On the LISA science performance in observations of short-lived signals from massive black hole binary coalescences,” (2022), [arXiv:2212.02572 \[gr-qc\]](#).
- [84] Theocharis A. Apostolatos, Curt Cutler, Gerald J. Sussman, and Kip S. Thorne, “Spin induced orbital precession and its modulation of the gravitational wave forms from merging binaries,” *Phys. Rev. D* **49**, 6274–6297 (1994).
- [85] Lawrence E. Kidder, “Coalescing binary systems of compact objects to postNewtonian 5/2 order. 5. Spin effects,” *Phys. Rev. D* **52**, 821–847 (1995), [arXiv:gr-qc/9506022](#).
- [86] Curt Cutler *et al.*, “The Last three minutes: issues in gravitational wave measurements of coalescing compact binaries,” *Phys. Rev. Lett.* **70**, 2984–2987 (1993), [arXiv:astro-ph/9208005](#).
- [87] Katerina Chatziioannou, Neil Cornish, Antoine Klein, and Nicolas Yunes, “Spin-Precession: Breaking the Black Hole–Neutron Star Degeneracy,” *Astrophys. J. Lett.* **798**, L17 (2015), [arXiv:1402.3581 \[gr-qc\]](#).
- [88] Geraint Pratten, Patricia Schmidt, Riccardo Buscicchio, and Lucy M. Thomas, “Measuring precession in asymmetric compact binaries,” *Phys. Rev. Res.* **2**, 043096 (2020), [arXiv:2006.16153 \[gr-qc\]](#).
- [89] Antoine Klein, Philippe Jetzer, and Mauro Sereno, “Parameter estimation for coalescing massive binary black holes with LISA using the full 2PN gravitational waveform and spin-orbit precession,” *Phys. Rev. D* **80**, 064027 (2009), [arXiv:0907.3318 \[astro-ph.CO\]](#).
- [90] Geraint Pratten *et al.*, “Computationally efficient models for the dominant and subdominant harmonic modes of precessing binary black holes,” *Phys. Rev. D* **103**, 104056 (2021), [arXiv:2004.06503 \[gr-qc\]](#).
- [91] Cecilio García-Quirós *et al.*, “Multimode frequency-domain model for the gravitational wave signal from nonprecessing black-hole binaries,” *Phys. Rev. D* **102**, 064002 (2020), [arXiv:2001.10914 \[gr-qc\]](#).
- [92] Geraint Pratten *et al.*, “Setting the cornerstone for a family of models for gravitational waves from compact binaries: The dominant harmonic for nonprecessing quasicircular black holes,” *Phys. Rev. D* **102**, 064001 (2020), [arXiv:2001.11412 \[gr-qc\]](#).
- [93] Antoine Klein *et al.*, “The last three years: multiband gravitational-wave observations of stellar-mass binary black holes,” (2022), [arXiv:2204.03423 \[astro-ph.HE\]](#).
- [94] Alexandre Toubiana, Sylvain Marsat, Stanislav Babak, John Baker, and Tito Dal Canton, “Parameter estimation of stellar-mass black hole binaries with LISA,”

- Phys. Rev. D **102**, 124037 (2020), arXiv:2007.08544 [gr-qc].
- [95] Michael L. Katz, Jean-Baptiste Bayle, Alvin J. K. Chua, and Michele Vallisneri, “Assessing the data-analysis impact of LISA orbit approximations using a GPU-accelerated response model,” Phys. Rev. D **106**, 103001 (2022), arXiv:2204.06633 [gr-qc].
- [96] Matthew C. Digman and Neil J. Cornish, “Parameter Estimation for Stellar-Origin Black Hole Mergers In LISA,” (2022), arXiv:2212.04600 [gr-qc].
- [97] Tyson B. Littenberg and Neil J. Cornish, “Prototype global analysis of LISA data with multiple source types,” Phys. Rev. D **107**, 063004 (2023), arXiv:2301.03673 [gr-qc].
- [98] Sylvain Marsat and John G. Baker, “Fourier-domain modulations and delays of gravitational-wave signals,” (2018), arXiv:1806.10734 [gr-qc].
- [99] Antoine Klein, Neil Cornish, and Nicolás Yunes, “Fast Frequency-domain Waveforms for Spin-Precessing Binary Inspirals,” Phys. Rev. D **90**, 124029 (2014), arXiv:1408.5158 [gr-qc].
- [100] Antoine Klein, Neil Cornish, and Nicolás Yunes, “Gravitational waveforms for precessing, quasicircular binaries via multiple scale analysis and uniform asymptotics: The near spin alignment case,” Phys. Rev. D **88**, 124015 (2013), arXiv:1305.1932 [gr-qc].
- [101] Thomas A. Prince, Massimo Tinto, Shane L. Larson, and J. W. Armstrong, “The LISA optimal sensitivity,” Phys. Rev. D **66**, 122002 (2002), arXiv:gr-qc/0209039.
- [102] Massimo Tinto and Sanjeev V. Dhurandhar, “TIME DELAY,” Living Rev. Rel. **8**, 4 (2005), arXiv:gr-qc/0409034.
- [103] Riccardo Busicchio *et al.*, “Bayesian parameter estimation of stellar-mass black-hole binaries with LISA,” Phys. Rev. D **104**, 044065 (2021), arXiv:2106.05259 [astro-ph.HE].
- [104] Louis J. Rubbo, Neil J. Cornish, and Olivier Poujade, “Forward modeling of space borne gravitational wave detectors,” Phys. Rev. D **69**, 082003 (2004), arXiv:gr-qc/0311069.
- [105] John Skilling, “Nested sampling,” in *Aip conference proceedings*, Vol. 735 (American Institute of Physics, 2004) pp. 395–405.
- [106] John Skilling, “Nested sampling for general Bayesian computation,” Bayesian Analysis **1**, 833 – 859 (2006).
- [107] Joshua S. Speagle, “DYNESTY: a dynamic nested sampling package for estimating Bayesian posteriors and evidences,” Mon. Not. R. Astron. Soc. **493**, 3132–3158 (2020), arXiv:1904.02180 [astro-ph.IM].
- [108] Sergey Kozlov *et al.*, “joshspeagle/dynesty: v2.1.2,” (2023).
- [109] Curt Cutler and Éanna E. Flanagan, “Gravitational waves from merging compact binaries: How accurately can one extract the binary’s parameters from the inspiral waveform?” Phys. Rev. D **49**, 2658–2697 (1994), arXiv:gr-qc/9402014 [gr-qc].
- [110] LISA Science Study Team, *LISA Science Requirements Document, ESA-L3-EST-SCI-RS-001*, Tech. Rep. 1.0 (ESA, 2018).
- [111] LISA Science Study Team, *LISA Science Requirements Document*, Tech. Rep. ESA-L3-EST-SCI-RS-001 (LISA, 2018).
- [112] Stanislav Babak *et al.*, “Science with the space-based interferometer LISA. V: Extreme mass-ratio inspirals,” Phys. Rev. D **95**, 103012 (2017), arXiv:1703.09722 [gr-qc].
- [113] Matthew C. Edwards *et al.*, “Identifying and Addressing Nonstationary LISA Noise,” Phys. Rev. D **102**, 084062 (2020), arXiv:2004.07515 [gr-qc].
- [114] B. M. Barker and R. F. O’Connell, “Derivation of the equations of motion of a gyroscope from the quantum theory of gravitation,” Phys. Rev. D **2**, 1428–1435 (1970).
- [115] B. M. Barker and R. F. O’Connell, “Gravitational Two-Body Problem with Arbitrary Masses, Spins, and Quadrupole Moments,” Phys. Rev. D **12**, 329–335 (1975).
- [116] Thibault Damour, “Coalescence of two spinning black holes: an effective one-body approach,” Phys. Rev. D **64**, 124013 (2001), arXiv:gr-qc/0103018.
- [117] Etienne Racine, “Analysis of spin precession in binary black hole systems including quadrupole-monopole interaction,” Phys. Rev. D **78**, 044021 (2008), arXiv:0803.1820 [gr-qc].
- [118] P. Ajith *et al.*, “Inspirals-mergers-ringdown waveforms for black-hole binaries with non-precessing spins,” Phys. Rev. Lett. **106**, 241101 (2011), arXiv:0909.2867 [gr-qc].
- [119] Davide Gerosa *et al.*, “A generalized precession parameter  $\chi_p$  to interpret gravitational-wave data,” Phys. Rev. D **103**, 064067 (2021), arXiv:2011.11948 [gr-qc].
- [120] B. P. Abbott *et al.* (LIGO Scientific, Virgo), “GWTC-1: A Gravitational-Wave Transient Catalog of Compact Binary Mergers Observed by LIGO and Virgo during the First and Second Observing Runs,” Phys. Rev. X **9**, 031040 (2019), arXiv:1811.12907 [astro-ph.HE].
- [121] R. Abbott *et al.* (LIGO Scientific, Virgo), “GWTC-2: Compact Binary Coalescences Observed by LIGO and Virgo During the First Half of the Third Observing Run,” Phys. Rev. X **11**, 021053 (2021), arXiv:2010.14527 [gr-qc].
- [122] R. Abbott *et al.* (LIGO Scientific, VIRGO, KAGRA), “GWTC-3: Compact Binary Coalescences Observed by LIGO and Virgo During the Second Part of the Third Observing Run,” (2021), arXiv:2111.03606 [gr-qc].
- [123] N. Aghanim *et al.* (Planck), “Planck 2018 results. VI. Cosmological parameters,” Astron. Astrophys. **641**, A6 (2020), [Erratum: Astron. Astrophys. 652, C4 (2021)], arXiv:1807.06209 [astro-ph.CO].
- [124] Michael L. Katz, Sylvain Marsat, Alvin J. K. Chua, Stanislav Babak, and Shane L. Larson, “GPU-accelerated massive black hole binary parameter estimation with LISA,” Phys. Rev. D **102**, 023033 (2020), arXiv:2005.01827 [gr-qc].
- [125] Patricia Schmidt, Frank Ohme, and Mark Hannam, “Towards models of gravitational waveforms from generic binaries II: Modelling precession effects with a single effective precession parameter,” Phys. Rev. D **91**, 024043 (2015), arXiv:1408.1810 [gr-qc].
- [126] Alberto Mangiagli, Chiara Caprini, Marta Volonteri, Sylvain Marsat, Susanna Vergani, Nicola Tamanini, and Henri Inchauspé, “Massive black hole binaries in LISA: Multimessenger prospects and electromagnetic counterparts,” Phys. Rev. D **106**, 103017 (2022), arXiv:2207.10678 [astro-ph.HE].
- [127] Leo P. Singer and Larry R. Price, “Rapid Bayesian position reconstruction for gravitational-wave transients,”

- Phys. Rev. D **93**, 024013 (2016), arXiv:1508.03634 [gr-qc].
- [128] LISA Science Study Team, *LISA Science Requirements Document, ESA-L3-EST-SCI-RS-001*, Tech. Rep. 1.0 (ESA, 2018).
- [129] Luciano Combi *et al.*, “Minidisk Accretion onto Spinning Black Hole Binaries: Quasi-periodicities and Outflows,” *Astrophys. J.* **928**, 187 (2022), arXiv:2109.01307 [astro-ph.HE].
- [130] Shihong Liao *et al.*, “Modelling the accretion and feedback of supermassive black hole binaries in gas-rich galaxy mergers,” *Mon. Not. Roy. Astron. Soc.* **520**, 4463 (2023), arXiv:2211.11788 [astro-ph.GA].
- [131] Mark J. Avara *et al.*, “Accretion onto a Supermassive Black Hole Binary Before Merger,” (2023), arXiv:2305.18538 [astro-ph.HE].
- [132] Alexander J. Dittmann, Geoffrey Ryan, and M. Coleman Miller, “The Decoupling of Binaries from Their Circumbinary Disks,” (2023), arXiv:2303.16204 [astro-ph.HE].
- [133] Davide Gerosa and Michael Kesden, “PRECESSION: Dynamics of spinning black-hole binaries with python,” *Phys. Rev. D* **93**, 124066 (2016), arXiv:1605.01067 [astro-ph.HE].
- [134] Davide Gerosa *et al.*, “Efficient multi-timescale dynamics of precessing black-hole binaries,” (2023), arXiv:2304.04801 [gr-qc].
- [135] Michael Kramer, “Determination of the geometry of the psr b1913+16 system by geodetic precession,” *Astrophys. J.* **509**, 856 (1998), arXiv:astro-ph/9808127.
- [136] Rene P. Breton *et al.*, “Relativistic Spin Precession in the Double Pulsar,” *Science* **321**, 104–107 (2008), arXiv:0807.2644 [astro-ph].
- [137] R. N. Manchester *et al.*, “Observations and Modelling of Relativistic Spin Precession in PSR J1141-6545,” *Astrophys. J.* **710**, 1694–1709 (2010), arXiv:1001.1483 [astro-ph.GA].
- [138] B. B. P. Perera *et al.*, “The Evolution of PSR J0737-3039B and a Model for Relativistic Spin Precession,” *Astrophys. J.* **721**, 1193–1205 (2010), arXiv:1008.1097 [astro-ph.GA].
- [139] Emmanuel Fonseca, Ingrid H. Stairs, and Stephen E. Thorsett, “A Comprehensive Study of Relativistic Gravity Using PSR B1534+12,” *Astrophys. J.* **787**, 82 (2014), arXiv:1402.4836 [astro-ph.HE].
- [140] WB Bonnor and MA Rotenberg, “Transport of momentum by gravitational waves: the linear approximation,” *Proceedings of the Royal Society of London. Series A. Mathematical and Physical Sciences* **265**, 109–116 (1961).
- [141] Asher Peres, “Classical radiation recoil,” *Phys. Rev.* **128**, 2471–2475 (1962).
- [142] Jacob D. Bekenstein, “Gravitational-Radiation Recoil and Runaway Black Holes,” *Astrophys. J.* **183**, 657–664 (1973).
- [143] M. J. Fitchett, “The influence of gravitational wave momentum losses on the centre of mass motion of a Newtonian binary system,” *Mon. Not. R. Astron. Soc.* **203**, 1049–1062 (1983).
- [144] Jose A. Gonzalez *et al.*, “Total recoil: The Maximum kick from nonspinning black-hole binary inspiral,” *Phys. Rev. Lett.* **98**, 091101 (2007), arXiv:gr-qc/0610154.
- [145] Manuela Campanelli, Carlos O. Lousto, Yosef Zlochower, and David Merritt, “Maximum gravitational recoil,” *Phys. Rev. Lett.* **98**, 231102 (2007), arXiv:gr-qc/0702133.
- [146] J. A. Gonzalez *et al.*, “Supermassive recoil velocities for binary black-hole mergers with antialigned spins,” *Phys. Rev. Lett.* **98**, 231101 (2007), arXiv:gr-qc/0702052.
- [147] Frank Herrmann *et al.*, “Gravitational recoil from spinning binary black hole mergers,” *Astrophys. J.* **661**, 430–436 (2007), arXiv:gr-qc/0701143.
- [148] Carlos O. Lousto and Yosef Zlochower, “Hangup Kicks: Still Larger Recoils by Partial Spin/Orbit Alignment of Black-Hole Binaries,” *Phys. Rev. Lett.* **107**, 231102 (2011), arXiv:1108.2009 [gr-qc].
- [149] Vijay Varma, Maximiliano Isi, and Sylvia Biscoveanu, “Extracting the Gravitational Recoil from Black Hole Merger Signals,” *Phys. Rev. Lett.* **124**, 101104 (2020), arXiv:2002.00296 [gr-qc].
- [150] Vijay Varma *et al.*, “Evidence of Large Recoil Velocity from a Black Hole Merger Signal,” *Phys. Rev. Lett.* **128**, 191102 (2022), arXiv:2201.01302 [astro-ph.HE].
- [151] David Merritt, Milos Milosavljevic, Marc Favata, Scott A. Hughes, and Daniel E. Holz, “Consequences of gravitational radiation recoil,” *Astrophys. J. Lett.* **607**, L9–L12 (2004), arXiv:astro-ph/0402057.
- [152] S. Komossa and David Merritt, “Gravitational Wave Recoil Oscillations of Black Holes: Implications for Unified Models of Active Galactic Nuclei,” *Astrophys. J. Lett.* **689**, L89 (2008), arXiv:0811.1037 [astro-ph].
- [153] Laura Blecha *et al.*, “Recoiling Black Holes in Merging Galaxies: Relationship to AGN Lifetimes, Starbursts, and the M-sigma Relation,” *Mon. Not. Roy. Astron. Soc.* **412**, 2154 (2011), arXiv:1009.4940 [astro-ph.CO].
- [154] I. H. Redmount and M. J. Rees, “Gravitational-radiation rocket effects and galactic structure.” *Comments on Astrophysics* **14**, 165 (1989).
- [155] Marta Volonteri, Kayhan Gültekin, and Massimo Dotti, “Gravitational recoil: effects on massive black hole occupation fraction over cosmic time,” *Mon. Not. R. Astron. Soc.* **404**, 2143–2150 (2010), arXiv:1001.1743 [astro-ph.CO].
- [156] Davide Gerosa and Alberto Sesana, “Missing black holes in brightest cluster galaxies as evidence for the occurrence of superkicks in nature,” *Mon. Not. Roy. Astron. Soc.* **446**, 38–55 (2015), arXiv:1405.2072 [astro-ph.GA].
- [157] A. sesana, “Extreme recoils: impact on the detection of gravitational waves from massive black hole binaries,” *Mon. Not. Roy. Astron. Soc.* **382**, 6 (2007), arXiv:0707.4677 [astro-ph].
- [158] A. Sesana, M. Volonteri, and F. Haardt, “LISA detection of massive black hole binaries: imprint of seed populations and of extreme recoils,” *Class. Quant. Grav.* **26**, 094033 (2009), arXiv:0810.5554 [astro-ph].
- [159] Milos Milosavljevic and E. S. Phinney, “The Afterglow of massive black hole coalescence,” *Astrophys. J. Lett.* **622**, L93–L96 (2005), arXiv:astro-ph/0410343.
- [160] Sean M. O’Neill *et al.*, “Reaction of Accretion Disks to Abrupt Mass Loss During Binary Black Hole Merger,” *Astrophys. J.* **700**, 859–871 (2009), arXiv:0812.4874 [astro-ph].
- [161] Jeremy D. Schnittman and Julian H. Krolik, “The Infrared Afterglow of Supermassive Black Hole Mergers,” *Astrophys. J.* **684**, 835–844 (2008), arXiv:0802.3556 [astro-ph].
- [162] Zoltan Lippai, Zsolt Frei, and Zoltan Haiman, “Prompt Shocks in the Gas Disk Around a Recoiling Supermas-

- sive Black Hole Binary,” *Astrophys. J. Lett.* **676**, L5 (2008), [arXiv:0801.0739 \[astro-ph\]](#).
- [163] Miguel Megevand *et al.*, “Perturbed disks get shocked: Binary black hole merger effects on accretion disks,” *Phys. Rev. D* **80**, 024012 (2009).
- [164] Elena M. Rossi *et al.*, “Black hole mergers: the first light,” *Mon. Not. R. Astron. Soc.* **401**, 2021–2035 (2010), [arXiv:0910.0002 \[astro-ph.HE\]](#).
- [165] S. Komossa, “Recoiling black holes: electromagnetic signatures, candidates, and astrophysical implications,” *Adv. Astron.* **2012**, 364973 (2012), [arXiv:1202.1977 \[astro-ph.CO\]](#).
- [166] L. Piro *et al.*, “Chasing Super-Massive Black Hole merging events with *Athena* and LISA,” *Mon. Not. Roy. Astron. Soc.* **521**, 2577–2592 (2023), [arXiv:2211.13759 \[astro-ph.HE\]](#).
- [167] Vijay Varma *et al.*, “High-accuracy mass, spin, and recoil predictions of generic black-hole merger remnants,” *Phys. Rev. Lett.* **122**, 011101 (2019), [arXiv:1809.09125 \[gr-qc\]](#).
- [168] Gabriella Agazie *et al.* (NANOGrav), “The NANOGrav 15 yr Data Set: Evidence for a Gravitational-wave Background,” *Astrophys. J. Lett.* **951**, L8 (2023), [arXiv:2306.16213 \[astro-ph.HE\]](#).
- [169] Gabriella Agazie *et al.* (NANOGrav), “The NANOGrav 15-year Data Set: Constraints on Supermassive Black Hole Binaries from the Gravitational Wave Background,” (2023), [arXiv:2306.16220 \[astro-ph.HE\]](#).
- [170] J. Antoniadis *et al.*, “The second data release from the European Pulsar Timing Array I. The dataset and timing analysis,” (2023), [10.1051/0004-6361/202346841, arXiv:2306.16224 \[astro-ph.HE\]](#).
- [171] J. Antoniadis *et al.*, “The second data release from the European Pulsar Timing Array III. Search for gravitational wave signals,” (2023), [arXiv:2306.16214 \[astro-ph.HE\]](#).
- [172] J. Antoniadis *et al.*, “The second data release from the European Pulsar Timing Array: V. Implications for massive black holes, dark matter and the early Universe,” (2023), [arXiv:2306.16227 \[astro-ph.CO\]](#).
- [173] Daniel J. Reardon *et al.*, “Search for an Isotropic Gravitational-wave Background with the Parkes Pulsar Timing Array,” *Astrophys. J. Lett.* **951**, L6 (2023), [arXiv:2306.16215 \[astro-ph.HE\]](#).
- [174] Heng Xu *et al.*, “Searching for the Nano-Hertz Stochastic Gravitational Wave Background with the Chinese Pulsar Timing Array Data Release I,” *Res. Astron. Astrophys.* **23**, 075024 (2023), [arXiv:2306.16216 \[astro-ph.HE\]](#).
- [175] Nathan Steinle *et al.*, “Implications of pulsar timing array observations for LISA detections of massive black hole binaries,” (2023), [arXiv:2305.05955 \[astro-ph.HE\]](#).
- [176] Mohammed Khalil *et al.*, “Theoretical groundwork supporting the precessing-spin two-body dynamics of the effective-one-body waveform models SEOBNRv5,” (2023), [arXiv:2303.18143 \[gr-qc\]](#).
- [177] Antoni Ramos-Buades *et al.*, “SEOBNRv5PHM: Next generation of accurate and efficient multipolar precessing-spin effective-one-body waveforms for binary black holes,” (2023), [arXiv:2303.18046 \[gr-qc\]](#).
- [178] Lorenzo Pompili *et al.*, “Laying the foundation of the effective-one-body waveform models SEOBNRv5: improved accuracy and efficiency for spinning non-precessing binary black holes,” (2023), [arXiv:2303.18039 \[gr-qc\]](#).
- [179] Maarten van de Meent *et al.*, “Enhancing the SEOBNRv5 effective-one-body waveform model with second-order gravitational self-force fluxes,” (2023), [arXiv:2303.18026 \[gr-qc\]](#).
- [180] Hang Yu *et al.*, “IMRPhenomXODE: An Accurate and Efficient Waveform Model for Precessing Binary Black Holes,” (2023), [arXiv:2306.08774 \[gr-qc\]](#).
- [181] Eleanor Hamilton *et al.*, “Model of gravitational waves from precessing black-hole binaries through merger and ringdown,” *Phys. Rev. D* **104**, 124027 (2021), [arXiv:2107.08876 \[gr-qc\]](#).
- [182] Barry Wardell *et al.*, “Gravitational Waveforms for Compact Binaries from Second-Order Self-Force Theory,” *Phys. Rev. Lett.* **130**, 241402 (2023), [arXiv:2112.12265 \[gr-qc\]](#).
- [183] Enrico Barausse and Luciano Rezzolla, “The Influence of the hydrodynamic drag from an accretion torus on extreme mass-ratio inspirals,” *Phys. Rev. D* **77**, 104027 (2008), [arXiv:0711.4558 \[gr-qc\]](#).
- [184] Bence Kocsis, Nicolas Yunes, and Abraham Loeb, “Observable Signatures of EMRI Black Hole Binaries Embedded in Thin Accretion Disks,” *Phys. Rev. D* **84**, 024032 (2011), [arXiv:1104.2322 \[astro-ph.GA\]](#).
- [185] Enrico Barausse, Vitor Cardoso, and Paolo Pani, “Can environmental effects spoil precision gravitational-wave astrophysics?” *Phys. Rev. D* **89**, 104059 (2014), [arXiv:1404.7149 \[gr-qc\]](#).
- [186] Lorenzo Speri *et al.*, “Probing Accretion Physics with Gravitational Waves,” *Phys. Rev. X* **13**, 021035 (2023), [arXiv:2207.10086 \[gr-qc\]](#).
- [187] Lorenz Zwick, Pedro R. Capelo, and Lucio Mayer, “Priorities in gravitational waveforms for future spaceborne detectors: vacuum accuracy or environment?” *Mon. Not. Roy. Astron. Soc.* **521**, 4645–4651 (2023), [arXiv:2209.04060 \[gr-qc\]](#).
- [188] Neil J. Cornish, “Heterodyned likelihood for rapid gravitational wave parameter inference,” *Phys. Rev. D* **104**, 104054 (2021), [arXiv:2109.02728 \[gr-qc\]](#).
- [189] Nathaniel Leslie, Liang Dai, and Geraint Pratten, “Mode-by-mode relative binning: Fast likelihood estimation for gravitational waveforms with spin-orbit precession and multiple harmonics,” *Phys. Rev. D* **104**, 123030 (2021), [arXiv:2109.09872 \[astro-ph.IM\]](#).
- [190] Geraint Pratten *et al.*, (In Prep.).
- [191] Geraint Pratten *et al.*, (In Prep.).
- [192] Charles R. Harris *et al.*, “Array programming with NumPy,” *Nature* **585**, 357–362 (2020).
- [193] J. D. Hunter, “Matplotlib: A 2d graphics environment,” *Computing in Science & Engineering* **9**, 90–95 (2007).
- [194] Pauli Virtanen *et al.*, “SciPy 1.0: Fundamental Algorithms for Scientific Computing in Python,” *Nature Methods* **17**, 261–272 (2020).
- [195] Antony Lewis, “GetDist: a Python package for analysing Monte Carlo samples,” (2019), [arXiv:1910.13970 \[astro-ph.IM\]](#).